Hindawi
Structural Control and Health Monitoring
Volume 2024, Article ID 6860185, 36 pages
https://doi.org/10.1155/2024/6860185

Review Article

Magnetorheological Fluid Dampers: A Close Look at Efficient Parametric Models

Arash Bahar[1], **Francesc Pozo**[2,3], **Mehdi Rashidi Meybodi**[1] and **Saeed Karami**[1]

[1]*Faculty of Engineering, Department of Civil Engineering, University of Guilan, Rasht, Iran*
[2]*Control, Data and Artificial Intelligence (CoDAlab), Department of Mathematics, Escola d'Enginyeria de Barcelona Est (EEBE), Universitat Politècnica de Catalunya (UPC), Campus Diagonal-Besòs (CDB), Eduard Maristany, 16, Barcelona 08019, Spain*
[3]*Institute of Mathematics (IMTech), Universitat Politècnica de Catalunya (UPC), Barcelona, Spain*

Correspondence should be addressed to Arash Bahar; bahar@guilan.ac.ir

Received 28 January 2023; Revised 20 November 2023; Accepted 20 December 2023; Published 16 January 2024

Academic Editor: Tzu-Kang Lin

The reasonable efficiency, high reliability, and minimal maintenance requirements of the semiactive control algorithms make this form of structural control the most successful method from a practical point of view. In addition, significant progress has been made in structural control devices. Magnetorheological (MR) dampers have been the subject of extensive research. In order to develop and implement a successful structural control algorithm, a deep understanding of their operation is required. Therefore, many efforts have been made to classify MR dampers as efficient tools; however, their complicated behavior has also been noted. Various relations have been proposed to describe the highly nonlinear behavior of MR dampers. To develop an efficient control algorithm, one must first properly understand the seismic behavior of the structure and the control device as well as its handling. The handling of the device will be efficient if there is a description for its control, a so-called inverse model. This model is an answer to the question of whether the proposed device model can be written in a form that practically brings the generated damping force as close as possible to the desired force. In the identification process, the selection of a basic mathematical model is critical. In this review article, we have compiled successful parametric models that accurately replicate the behavior of MR dampers. Since the primary functionality of the device is crucial for the development of a competent control algorithm, we have endeavored to investigate and present the reversibility of the proposed models. We also delved at the characteristics of the parameters that enable precise communication between the central control unit and the device. These parameters, which enable the dialog between the processing unit and the control devices, will play an important role in the development of the inverse model in its simplicity and efficiency.

1. Introduction

One of the ongoing challenges in civil engineering is the protection of facilities from destructive forces caused by wind and earthquakes. The traditional seismic design assumes that an earthquake acts on a building through a solid base. To ensure partial dissipation of the induced energy, plastic deformation occurs in certain building components and structural damage occurs to some extent. This drawback can be avoided using structural control strategies. The concept of control applications for improving the seismic performance of structures has been considered for several years. Passive supplemental damping strategies are well known and widely accepted by engineers for mitigating the effects of dynamic loading on structures [1–4]. However, preliminary studies indicate that appropriately implemented semiactive systems perform significantly better than passive devices and have the potential to achieve most of the performance outcomes of fully active systems. This enables an effective reduction in responses under a wide range of dynamic loading conditions. The reasonable efficiency, high reliability, and minimal maintenance requirements of semiactive control algorithms render this form of structural control, the most successful method in terms of theoretical and practical considerations. Additionally, significant advances have been made in structural control devices. Among

these, dampers, particularly magnetorheological (MR) dampers, appear to have significant potential to advance the acceptance of structural control as a viable means of mitigating dynamic hazards and have accounted for a large portion of studies in this area.

Jacob Rainbow [5] developed an MR fluid smart material in the 1940s. An MR damper comprises this solution, which can reversibly transform from a free-flowing linear viscous fluid to a semisolid with a controllable yield point in the presence of a magnetic field [6]. This feature provides simple, quiet, and responsive interfaces between the electronic controls and mechanical systems. Typically, MR fluids flow freely with a consistency similar to that of a motor oil [7]. However, in the presence of an applied magnetic field, iron particles (carbonyl iron) acquire a dipole moment aligned with the external magnetic field, causing them to form linear chains parallel to the field. This phenomenon solidifies suspended iron particles and restricts the motion of the liquid. Consequently, the yield strength develops within the fluid. This change is reflected in the change in the damping force when MR fluids are used. The magnitude of the change depends on the strength of the applied magnetic field and can occur within a few milliseconds.

Unlike their electrical counterparts' electrorheological (ER) fluids, MR fluids are not extremely sensitive to moisture or other contaminants that may arise during their manufacture and use [8, 9]. Because the mechanism of magnetic polarization is not affected by temperature, the performance of devices based on MR is relatively insensitive to temperature over a wide range of temperatures (including automotive use) [7]. Magnetorheological fluids can be used in three ways, all of which can be applied to MR devices depending on the intended use of the damper. These modes of operation are referred to as pinch, valve (pressure-controlled flow), and shear modes. The last mode of operation of the MR steamer, the valve mode, is the most commonly used among the three modes [10]. An MR device operates in the valve mode when the MR fluid is used to impede its flow from one reservoir to another. Most devices that use controllable fluids can be classified as either fixed-pole devices (which often operate in pressure-controlled flow mode) or relatively movable-pole devices (which operate in direct shear mode) [10].

The commercialization of MR technology began in 1995, with the use of rotational brakes in aerobic equipment. Since then, the application of MR material technology to actual systems has steadily increased [11]. Magnetorheological fluids operating in the valve mode with fixed magnetic poles are suitable for hydraulic controls, servo valves, shock absorbers, and dampers (including models referred to as tubular/linear MR dampers). The direct shear mode with a moving pole is suitable for clutches and brakes, clamping/locking devices, dampers (including models referred to as the shear mode or rotating MR dampers), breakaway devices, and structural composites [9].

In recent years, several commercially available products have been developed or are close to commercialization [12, 13]:

(i) MR dampers for real-time active control systems in heavy duty trucks

(ii) Linear and rotary brakes for low-cost, accurate, positional, and velocity control of pneumatic actuator systems

(iii) Rotary brakes to provide tactile force-feedback in steer-by wire systems

(iv) Linear dampers for real-time gait control in advanced prosthetic devices

(v) Adjustable real-time controlled shock absorbers for automobiles

(vi) MR sponge dampers for washing machines

(vii) Magnetorheological fluid polishing tools

(viii) Large MR fluid dampers to control wind-induced vibrations in cable-stayed bridges

(ix) Very large MR fluid dampers for seismic damage mitigation in civil engineering structures

Magnetorheological dampers provide an attractive solution for energy absorption in structures and considered fail-safe devices and are inexpensive [6], have few moving parts, and are reliable. These characteristics render MR dampers promising voltage- or current-controlled actuators that can be used in various engineering applications [7, 14]. In civil engineering applications, the expected damping forces are considerably high. For MR dampers, a memory-dependent multivalued relationship between force, deformation, and hysteresis is observed. Many mathematical models have been developed to efficiently describe this behavior and use them for time history and random vibration analysis. High-precision models for MR dampers can be developed using two families of models: semiphysical [15, 16] and black-box models [17, 18]. Semiphysical models use a simplified model of the physical device and thereafter use some type of measurement to identify its free parameters. The black-box model, on the other hand, is a strategy for studying a complex object or device without any knowledge or assumptions about its internal structure, parts, or model. Although some quasistatic models have been proposed and shown to describe the force-displacement relationship of the MR damper reasonably well, they have not been able to model its nonlinear force-velocity behavior.

More accurate dynamic models have been developed and can be divided into two categories: nonparametric and parametric. Nonparametric models are based solely on the performance of the device and typically require a large amount of experimental data to show the response of the fluid to various loads under different operating conditions. These proposed models are based on Chebyshev polynomials [19–21], neural networks [22–24], and neuro-fuzzy systems [25–27]. Neural networks can accurately reproduce the nonlinear behavior of MR fluids. However, since there is no specific mathematical expression for nonparametric models, the information obtained from the laboratory results must be examined in the form of complex cognitive methods to achieve acceptable accuracy with the neural

network method. In order to obtain appropriate results, the data set must be subjected to strict conditions. In addition, part of the data is always used to learn the model. On the other hand, the sensitivity of nonparametric models to interference from laboratory methods and sensors is low and one can work with different data sources, including real-world data collection under less controlled conditions. Multilayer perceptron (MLP) networks are one of the most commonly used neural network types and have the distinction of using only a single nonlinear function. They have also been shown to model both simple and complex systems accurately. Neuro-fuzzy models are another example of nonparametric models that have been proposed to emulate the behavior of MR dampers. Because these devices are highly nonlinear, fuzzy logic has been proposed as an alternative to the computationally intensive models that are currently in use. Neural networks were subsequently used to fit the fuzzy logic parameters. Fuzzy logic incorporates human knowledge about the system into the controller using membership functions, which are quantities that define imprecise or vague concepts, such as large, weak, hard, and moderate. The desired output is determined based on fuzzy information of the inputs, similar to how the human brain makes decisions. Although several nonparametric models can effectively reproduce the behavior of MR dampers, their application is often hindered by their complexity and the large amount of experimental data required for training and model validation. Therefore, parametric models are more commonly employed in simulations and in the development of control algorithms.

The objective of this study is to compile and present the most successful parametric models for this type of damper. In this study, we delve into models that are typically the most fitting parametric types, having undergone revisions throughout various research and testing phases. Grasping the evolution process, the interrelated combinations, and the role of each component in delivering the damping force offers a valuable guide. This insight can help propel research forward, culminating in more comprehensive relationships that align with the intricate and highly nonlinear behavior of this damper series.

Our research primarily concentrates on the potential and competence of the final model, especially its capability to yield an inverted model. The significance of indicator models is underscored. While developing some of these models, the dependency of the model on a governing parameter, namely, its interaction with the device, was also taken into account and discussed. From this vantage point, this research proves invaluable for researchers aiming to choose an apt model for their control structure design. Notably, each model can be rationally associated with one of the standard variables (either current or voltage) used in the damper during the tool's identification process. The precision and the researchers' emphasis on this aspect are accentuated in our study.

On the other hand, there are only a handful of models that rely on the frequency of stimulation during the identification phase. The dependence of the damper model on the frequency of the external stimuli is an aspect that is complicated in practical application. The vibrational properties of earthquakes themselves are very complex and extensive in terms of their variety and frequency content. Moreover, from a practical point of view, it is unsuitable to determine this content during an earthquake. So, there is no simple practical method to find out how much this frequency content influences the results. Therefore, this dependence model is limited to a small number in this overview and there is no separate section for them.

To streamline access to these models, reference is made to Table 1. This table lists the model name, the relation number mentioned in the text, its reversibility, and the kind of governing parameters. As observed, there are select models that, in addition to meeting reversibility criteria, can replicate precise numerical results pivotal for devising a suitable control algorithm for structural applications.

2. Dynamic Models Based on the Bingham Model

This group of modelers used the stress-strain diagram of the Bingham viscoplastic model [28] to describe the behavior of MR fluids. Based on the viscoplastic model, when the stress is greater than the field-dependent yield stress, the damper fluid can be represented by the Bingham equation as follows:

$$\tau = \tau_y + \eta\dot{\gamma}, \tag{1}$$

where η is the viscosity of the fluid and $\dot{\gamma}$ is the shear strain rate. The material behaved viscoelastically when the stress was lower than the yield stress. Many researchers based their modified version of the damper on this model.

2.1. Bingham Standard Model. Spencer et al. [16] proposed an idealized mechanical model used by Stanway et al. [29] to express the behavior of an ER damper based on the model described in (1). This model consists of a Coulomb friction element parallel to the viscous segment, as shown in Figure 1.

In this rigid viscoplastic model, the force generated by the damper is given by the following equation:

$$F = f_c \operatorname{sgn}(\dot{x}) + c_0\dot{x} + f_0, \tag{2}$$

where $\dot{x}$, c_0, and f_c denote the piston velocity, damping coefficient, and frictional force, respectively. f_0 is the offset in the resulting damping force owing to the accumulator. This model describes only the force-displacement behavior of the MR damper; however, it cannot accurately represent the force-velocity behavior, particularly in the roll-off region.

2.2. Gamota and Filisko Model. Gamota and Filisko [30] proposed an extension to the Bingham model for ER fluids (Figure 2). Spencer et al. [16] used the viscoelastic-plastic model for MR dampers. This model consists of a classical Bingham model connected to the Kelvin–Voigt representation of a standard linear solid model, also known as the Zener model (with two springs and a dashpot). In the Zener

Table 1: General information about the models mentioned in the text.

	Model's name/number of parameters	Formula	Inversable	Parameter's dependency
Bingham dynamic models	Bingham standard model/3	(2)	—	—
	Gamota and Filisko/6	(3)	—	—
	Bingham plastic/2	(5)	—	—
	Modified Bingham/4	(6)	—	—
	Improved Bingham/4	(9)	—	Current
	Nonlinear Bingham hysteretic/6	(10)	—	Current
	Hysteresis regularized Bingham model/5	(13)	—	—
Bouc–Wen hysteresis dynamic models	Standard Bouc–Wen model/7	(15), (16)	—	Potentially current or voltage
	Modified Bouc–Wen (phenomenological)/9	(17)	—	Current
	Bouc–Wen model in shear-mode/6	(15), (22)	—	Potentially on current
	Mass included Bouc–Wen/11, 8, 3,	(23), (25) or (26)	—	Potentially on current
	Amplitude-dependent Bouc–Wen/22	(16), (27)	—	Amplitude and current
	Current-dependent Bouc–Wen/13	(28), (30)	—	Comprehensive dependency on current
	Current-frequency-amplitude-dependent model/34	(31)	—	Current-frequency-amplitude
	Asymmetric sigmoid modified Bouc–Wen/12	(17), (33)	—	Current
	Nonsymmetrical Bouc–Wen/8	(35), (36)	—	Potentially current
	Normalized Bouc–Wen I/11	(40), (41)	—	—
	Modified normalized Bouc–Wen/27	(43)–(45)	Yes	Voltage
	Normalized Bouc–Wen II/11	(49), (48), or (50)	—	Current
	Normalized phenomenological model/8	(17), (51)	—	—
	Bai restructured model/8	(52)	—	—
LuGre	Original LuGre/4	(53)	—	—
	Modified LuGre/4	(54), (55)	Yes	Voltage
Biviscous	Nonlinear biviscous model/3	(56)	—	—
	Nonlinear hysteretic biviscous model/3	(57)	—	—
	Nonlinear hysteretic arctangent model/4	(58)	—	—
	Lumped-parameter fluid-flow model/9	(59)	—	Current
Viscoelastic-plastic	Nonlinear viscoelastic-plastic model/6	(69)	—	—
	Wereley viscoelastic-plastic model/5	(70)	—	—
	Li viscoelastic-plastic model/6	(73), (74)	Yes	—
	Continuous viscoelastic-plastic (VEP)/5	(77)	—	—
	Nonlinear stiffness VEP model (nkVEP)/15	(78), (79)	—	Current
	Stiffness-viscosity-elasto-slide (SVES) model/6	(80), (81)	—	—
Algebraic	Weng model/5	(82)	—	Potentially on current
	Cesmeci and Engin model/6	(83)	—	—
	Metered model/9	(84)	—	—
	Balamurgan model/11	(86)	—	Voltage

Table 1: Continued.

	Model's name/number of parameters	Formula	Inversable	Parameter's dependency
Hyper-tangent	Bass model/7	(87), (88)	—	Current
	Kwok model/7	(89)	Yes	Potentially on current
	Yang model/5, 6,	(90) or (91)	—	Current
	Cheng model/4	(92)	Yes	Current-frequency-amplitude
	Magic formula/8	(94)	Yes	Current
Dahl	Dahl model/2	(97)	—	—
	Modified Dahl/5	(98)	—	Potentially on voltage
	Viscous Dahl model/5	(99), (41)	—	Voltage
	Asymmetric Dahl/7	(99), (100)	—	Potentially on voltage
	General dynamic models/5 ~ 11	(101)–(106)	—	—

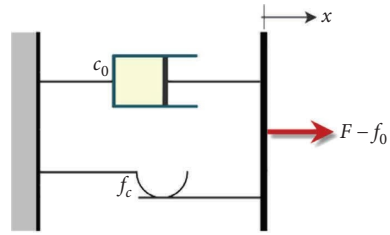

Figure 1: Bingham model (Section 2.1).

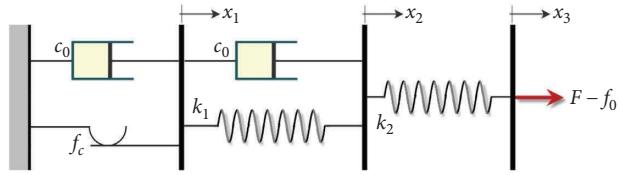

Figure 2: Gamota and Filisko model (Section 2.2).

model, the Kelvin representation is preferred over the Maxwell representation to demonstrate linear viscoelastic behavior in the preyield region. The following equations are associated with this model:

$$F = \begin{cases} k_1(x_2 - x_1) + c_1(\dot{x}_2 - \dot{x}_1) + f_0 = c_0\dot{x}_1 + f_c\mathrm{sgn}(\dot{x}_1) + f_0 = k_2(x_3 - x_2) + f_0, & |F| > f_c, \\ k_1(x_2 - x_1) + c_1(\dot{x}_2) + f_0 = k_2(x_3 - x_2) + f_0, & |F| \le f_c, \end{cases} \tag{3}$$

where c_0 denotes the damping coefficient of the Bingham model. Parameters k_1, k_2, and c_1 are the stiffness and damping coefficients of the Zener model, respectively. Although this model is suitable for predicting the behavior of a damper, its use in numerical problems is difficult.

2.3. Bingham Plastic Model. By adding a yielding force F_y to the linear damping model, Werely et al. [31–33] introduced the Bingham plastic model, as shown in Figure 3, which is similar to the Bingham standard model (equation (2)). The equations describing the model are as follows:

$$F = \begin{cases} C_{\mathrm{post}}v + F_y, & v > 0, \\ -F_y < F < F_y, & v = 0, \\ C_{\mathrm{post}}v - F_y, & v < 0. \end{cases} \tag{4}$$

The Bingham plastic model is expressed as follows:

$$F = f_y\mathrm{sgn}(\dot{x}) + C_{\mathrm{post}}\dot{x}. \tag{5}$$

This model assumes that, in the preyield state, the materials are rigid and do not flow. The shaft velocity is zero if F is lower than F_y. The fluid flowed when the applied force exceeded F_y. Subsequently, the materials became Newtonian fluids with a nonzero yield stress. Although this model can accurately predict the force-displacement diagram and dissipated energy owing to the presence of the yield force, which is reminiscent of Coulomb friction, the force-velocity diagram of the MR damper is not correctly modeled. The behavior of the damper is displayed rigidly in the preyield area, which is termed the roll-off area.

2.4. Modified Bingham Model. Zhou [34] proposed the modified Bingham plastic model shown in Figure 4. This model consists of a standard Bingham model with a stiffened k_1. The equation of the model is as follows:

$$F = c_0\dot{x}_1 + f_c\mathrm{sgn}(\dot{x}_1) + f_0 = k_1(x - x_1). \tag{6}$$

2.5. Improved Bingham Model. Based on an experiment performed by Occhiuzzi et al. [35], they found that the standard Bingham model overestimates the viscous component of the force-displacement cycle for $i = 0\,A$ and underestimates it for $i = 2.5$ A, where i is the current of the MR coil. They offered a relation between the damping coefficient and the magnetic field of the damper, which finally led to a dependency on the current. The resulting modified Bingham model is as follows:

$$F = c(i)\dot{x} + \left[F_{y_{\min}} + \left(F_{y_{\max}} - F_{y_{\min}}\right)\frac{i}{i_{\max}}\right]\mathrm{sgn}(\dot{x}), \tag{7}$$

$F_{y_{\max}}$ and $F_{y_{\min}}$ are the maximum and minimum values of the plastic surfaces respectively, owing to the frictional force. Subsequently, Occhiuzzi et al. suggested a nonlinear relation

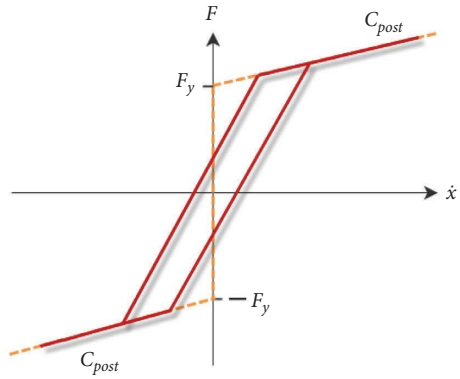

Figure 3: Bingham plastic model (Section 2.3).

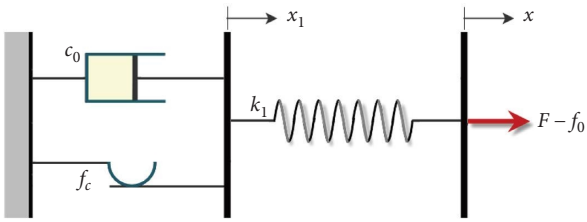

Figure 4: Modified Bingham model (Section 2.4).

between the viscous damping coefficient and the piston velocity of the damper, according to the following equation:

$$F_\eta = c(i)|\dot{x}|^{\alpha(i)}\operatorname{sgn}(\dot{x}), \tag{8}$$

where $c(i)$ and $\alpha(i)$ are current-dependent parameters. The final improved Bingham model can be obtained by integrating equations (7) and (8):

$$F = c(i)|\dot{x}|^{\alpha(i)}\operatorname{sgn}(\dot{x}) + \left[F_{y_{\min}} + \left(F_{y_{\max}} - F_{y_{\min}}\right)\frac{i}{i_{\max}}\right]\operatorname{sgn}(\dot{x}). \tag{9}$$

Because their experimental data did not show any trace of roll-off behavior, this model could not handle such an influence.

2.6. Nonlinear Bingham Hysteretic Model. Zhang and Huang [36] proposed a nonlinear hysteretic model for the Bingham model. At low velocities, this model can describe the hysteresis characteristics of the force-velocity diagram and the nonlinear behavior of the MR damper. The nonlinear Bingham hysteretic model (Figure 5) is given by

$$F = \begin{cases} kx_1 + \left(c_1|\dot{x}_2| + c_2|\dot{x}_2|^2\right)\dot{x}_2 + f_0, & |kx_1| \le F_y, \\ F_y\operatorname{sgn}(\dot{x}_2) + \left(c_0 + c_1|\dot{x}_2| + c_2|\dot{x}_2|^2\right)\dot{x}_2 + f_0, & |kx_1| \ge F_y, \end{cases} \tag{10}$$

where F_y denotes the yield force of the MR fluid; c_0, c_1, and c_2 are constant coefficients of the nonlinear damping term of the model; k denotes the equivalent stiffness of the model spring element; f_0 is the deviation force owing to the accumulator; and x_1 is the elongation of the spring, which is given by (11).

$$x_1 = \begin{cases} x_2 - \left|x_{2_{\max}} - \dfrac{F_y}{k}\right|, & \dot{x}_2 \le 0, \left|x_{2_{\max}} - x_2\right| \le \dfrac{2F_y}{k}, \\ x_2 + \left|x_{2_{\max}} + \dfrac{F_y}{k}\right|, & \dot{x}_2 \ge 0, \left|x_{2_{\max}} - x_2\right| \le \dfrac{2F_y}{k}, \\ \dfrac{F_y}{k}\operatorname{sgn}(\dot{x}_2), & \text{otherwise.} \end{cases} \tag{11}$$

The model variables are dependent on the applied current.

2.7. Hysteresis-Regularized Bingham Model. Using the standard Bingham model, Soltane et al. [37] proposed the hysteresis regularized Bingham model (HRB). They applied a regularization technique [38] to the discontinuous Bingham equation and converted it into a continuous relation as shown in Figure 6. Equation (12) shows the generated force of the MR damper, based on the following model:

$$F_d^{\mathrm{RB}} - F_0 = c_v\dot{x}_d + F_y\left[1 - \exp\left(-\operatorname{sgn}(\dot{x}_d)\frac{\dot{x}_d}{\dot{x}_0}\right)\right]\operatorname{sgn}(\dot{x}_d), \tag{12}$$

where $\dot{x}_0$, and together with the velocity dimension, is a regularization parameter that exponentially controls the growth of the damping force. Equation (12) is converted into (13) to consider the nonlinear hysteresis behavior of the MR damper.

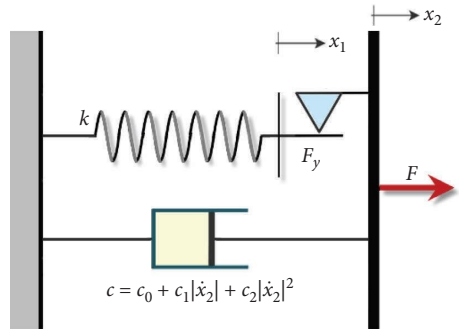

FIGURE 5: Nonlinear Bingham hysteretic model (Section 2.6).

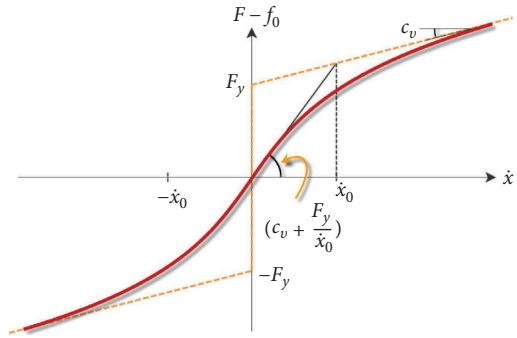

FIGURE 6: Hysteresis regularized Bingham model (Section 2.7).

$$F_d^{\mathrm{RB}} - F_0 = \begin{cases} c_v(\dot{x}_d - \dot{x}_h) + F_y\left[1 - \exp\left(-\mathrm{sgn}(\dot{x}_d - \dot{x}_h)\dfrac{\dot{x}_d - \dot{x}_h}{\dot{x}_0}\right)\right]\mathrm{sgn}(\dot{x}_d - \dot{x}_h)\,\dot{x}_d < 0, \\ c_v(\dot{x}_d + \dot{x}_h) + F_y\left[1 - \exp\left(-\mathrm{sgn}(\dot{x}_d + \dot{x}_h)\dfrac{\dot{x}_d + \dot{x}_h}{\dot{x}_0}\right)\right]\mathrm{sgn}(\dot{x}_d + \dot{x}_h)\,\dot{x}_d > 0, \end{cases} \tag{13}$$

where $\dot{x}_h$ is the scale factor, which has a velocity dimension and defines the width of the hysteresis loop. Dynamic Bingham models have been used to simulate the behavior of MR dampers in several studies. It is simple, effective, and numerically easy to handle. However, there is another group of models for these devices that is even more significant, which are described in the following sections.

3. Dynamic Models Based on the Bouc–Wen Hysteresis Operator

The Bouc–Wen model is widely used for modeling hysteretic systems. This model was first proposed by Bouc [39], which was subsequently generalized by Wen [18, 40]. It is extremely versatile and can represent a wide range of hysteresis behaviors in devices and materials. Therefore, they have been used to model MR dampers. The force generated by this model for a nonlinear hysteretic system is

$$F(x, \dot{x}) = g(x, \dot{x}) + \alpha z(x). \tag{14}$$

Function $g(x, \dot{x})$ is a nonhysteretic component that can include the elastic property and/or viscous behavior of the damper. x and $\dot{x}$ denote the displacement and velocity of the system, respectively. α is the scaling parameter for the hysteretic term of the model. z, the hysteretic component of the model that depends on the time-history of the displacement, is the core of the model and assumes the shape of the hysteresis loop. The evolutionary variable was obtained using the following equation:

$$\dot{z} = -\gamma|\dot{x}|z|z|^{n-1} - \beta\dot{x}|z|^n + A\dot{x}, \tag{15}$$

where γ, β, A, and n are key parameters that define the shape of the hysteresis loop.

3.1. Standard Bouc–Wen Model. Based on the Bouc–Wen model, Spencer et al. [16] proposed a new model consisting of three components, as shown in Figure 7. Equation (16) describes the force generated by the model.

$$F = c_0\dot{x} + k_0 x + \alpha z(x), \tag{16}$$

where c_0 is a constant parameter for the viscosity term; k_0 is the stiffness of the damper, which reflects the elastic phenomenon of the MR fluid; and z is the hysteretic parameter of the model, given by (15). This parameter represents the dynamic behavior of the device. x_0 is the initial displacement

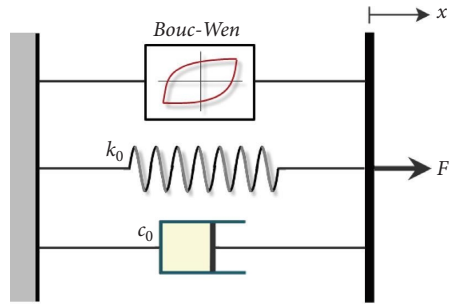

Figure 7: Standard Bouc–Wen model (Section 3.1).

of the piston, which was added to consider the effect of the accumulator. Dominguez et al. [41–43], Ambhore et al. [44], and Cézar and Baros [45] studied the effects of model parameters on the resulting hysteresis loop. This model has been widely used as an MR-damper model in several studies [46–48].

3.2. Modified Bouc–Wen (Phenomenological) Model. The standard Bouc–Wen model provides a good prediction of the force-displacement behavior of the damper; however, it does not perform well in describing the roll-off region of the force-velocity loop. To better predict the damper response in this region, a modified version of the model was proposed by Spencer et al. [16] as shown in Figure 8. The following equation describes the force generated by the model.

$$F = c_1\dot{y} + k_1 x,$$

$$\dot{y} = \frac{1}{c_0 + c_1}\left[\alpha z + c_0\dot{x} + k_0(x - y)\right], \tag{17}$$

$$\dot{z} = -\gamma|\dot{x} - \dot{y}|z|z|^{n-1} - \beta(\dot{x} - \dot{y})|z|^n + A(\dot{x} - \dot{y}).$$

In (17), k_1 is the accumulator stiffness; c_0 is the viscous damping parameter at high velocity; c_1 is the damping parameter of the dashpot added to the model to produce a roll-off effect at the low velocities; k_0 controls the overall stiffness of the device in a high-velocity situation; and x_0 denotes the initial displacement of the damper and produces an offset force when multiplied by k_1. This model has been used as an MR-damper model in extensive articles (for example, [49–53]). It must be mentioned that this model is referred to as the phenomenological model in many studies. For the proposed model to correctly predict the alternating behavior of the MR fluid under magnetic field changes, Spencer et al. [16] proposed a voltage-dependent linear relation for some of the parameters in the models as follows:

$$\begin{aligned}\alpha = \alpha(u) = \alpha_a + \alpha_b u;\ c_0 = c_0(u)\\ = c_{0a} + c_{0b}u;\ c_1 = c_1(u) = c_{1a} + c_{1b}u.\end{aligned} \tag{18}$$

In this relation, u is an intrinsic variable that relates the dependence of the parameters on the applied voltage and is calculated using the first-order filter as

$$\dot{u} = -\eta(u - v), \tag{19}$$

where v is the voltage applied to the current driver and η reflects the response time of the MR damper [16]. Assuming that the parameters of (18) are polynomials of the third degree, Yang et al. [54] performed a process of parameter identification and proposed a model for a large-scale MR damper. The suggested relations for the parameters are as follows:

$$\begin{aligned}\alpha(i) &= \alpha_a i^3 + \alpha_b i^2 + \alpha_c i + \alpha_d;\\ c_0(i) &= c_{0a} i^3 + c_{0b} i^2 + c_{0c} i + c_{0d};\\ c_1(i) &= c_{1a} i^3 + c_{1b} i^2 + c_{1c} i + c_{1d}.\end{aligned} \tag{20}$$

Spaggiari and Dragoni [55] studied the behavior of the damper at low frequencies. They modified the model by interpolating the parameters α, c_0, and c_1 based on the results of laboratory tests. The proposed quadratic polynomial functions for these parameters are as follows:

$$\begin{aligned}\alpha(i) &= \alpha_a i^2 + \alpha_b i + \alpha_c;\\ c_0(i) &= c_{0a} i^2 + c_{0b} i + c_{0c};\\ c_1(i) &= c_{1a} i^2 + c_{1b} i + c_{1c}.\end{aligned} \tag{21}$$

3.3. Bouc–Wen Model in the Shear-Mode MR Damper. Yi et al. [56] proposed a model for shear mode MR dampers established on the Bouc–Wen base model by Spencer et al. [16]. Spencer team damper was tubular in which MR fluid was sealed in a cylinder with a movable piston (see Figure 9).

In shear-mode dampers, the MR fluid is confined to the parallel plates. Figure 10(a) shows the schematic of this type of damper. The common models for these dampers consist of a viscous friction element and hysteretic component (see Figure 10(b)).

Equation (22) presents the force generated in this type of damper using the model [57–59].

$$F = c_0\dot{x} + \alpha z(x), \tag{22}$$

where z is the evolutionary variable given by (15).

3.4. Modified Bouc–Wen Model with Mass Element. This model, proposed by Yang et al. [60] for a large-scale MR damper, incorporates the MR fluid stiction phenomenon, as well as the effect of shear-thinning and fluid inertia. A

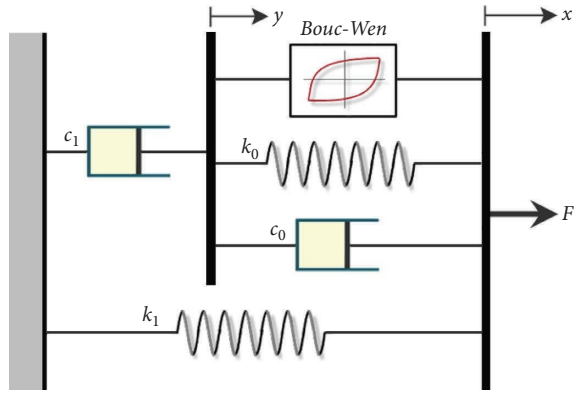

Figure 8: Modified Bouc–Wen model (Section 3.2).

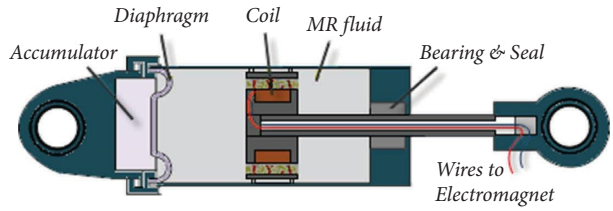

Figure 9: Common MR damper (Section 3.3).

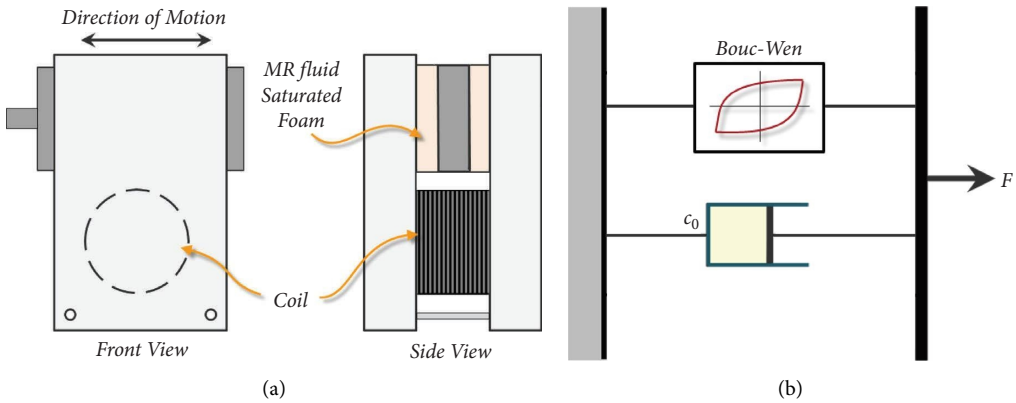

Figure 10: (a) Shear mode MR damper; (b) schematic of the device (Section 3.3).

schematic representation of the model is shown in Figure 11. The force generated by the damper is

$$F = m\ddot{x} + c_0(\dot{x})\dot{x} + kx + \alpha z(x) + f_0, \tag{23}$$

where m is equivalent mass which represents the MR fluid stiction phenomenon and inertial effect; k is accumulator stiffness and MR fluid compressibility; f_0 is the damper friction force due to seals and measurement bias; and $c_0(\dot{x})$ is the postyield plastic damping coefficient, which is defined as a monodecreasing function with respect to absolute velocity $\dot{x}$, to describe the MR fluid shear-thinning effect which results in the force roll-off of the damper resisting force in the low-velocity region. The postyield damping coefficient is given by the following equation:

$$c_0(\dot{x}) = a_1 e^{-(a_2|\dot{x}|)^p}, \tag{24}$$

where a_1, a_2, and p are positive constants. Lau and Liao [61, 62] and Tsampardoukas et al. [63] used this model in train and truck suspensions, respectively. Additionally, Yang et al. [60] presented two more dynamic models based on the standard Bouc–Wen form and the modified version updated with a mass element (Figure 12) [60].

According to Figure 7, the force generated by the damper in the standard Bouc–Wen model with the mass element is according to (25) and that for the modified Bouc–Wen model with the mass element is according to the following equations [60]:

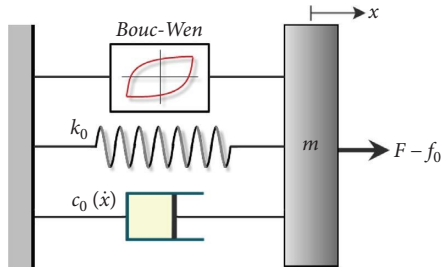

Figure 11: Modified Bouc–Wen model with mass element (Section 3.4).

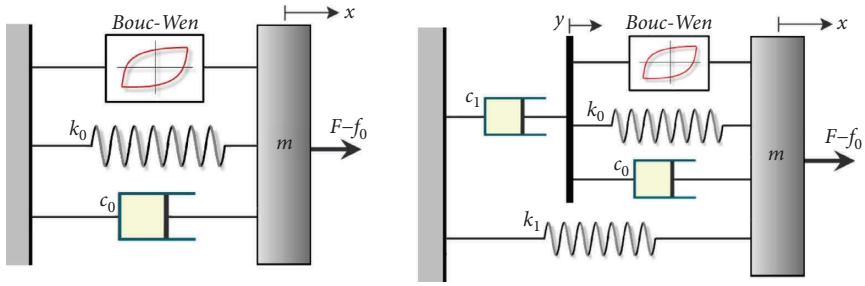

Figure 12: Additional models by Yang et al. [60] (Section 3.4).

$$F = m\ddot{x} + c_0\dot{x} + k_0 x + \alpha z, \tag{25}$$

$$F = m\ddot{x} + c_1\dot{y} + k_1 x. \tag{26}$$

The variables are defined in equations (15) and (17).

3.5. Amplitude-Dependent Bouc–Wen Model. Ali and Ramaswamy [64] proposed the amplitude-dependent Bouc–Wen model. In this model, the parameters c_0, k_0, and α expressed in (16) depend on the amplitude of excitation and the input current to the MR damper. The relationship between these parameters and the input current, i_c, changes linearly, and the effects of the motion amplitude are considered as a quadratic function of the stroke amplitude (x_a), as shown in the following equation:

$$\begin{aligned} c_0 &= \left(c_1 + c_2 x_a + c_3 x_a^2\right) + \left(c_4 + c_5 x_a + c_6 x_a^2\right) i_c, \\ k_0 &= \left(k_1 + k_2 x_a + k_3 x_a^2\right) + \left(k_4 + k_5 x_a + k_6 x_a^2\right) i_c, \\ \alpha_0 &= \left(\alpha_1 + \alpha_2 x_a + \alpha_3 x_a^2\right) + \left(\alpha_4 + \alpha_5 x_a + \alpha_6 x_a^2\right) i_c, \end{aligned} \tag{27}$$

where the parameters c_1, c_2, ..., α_5, and α_6 are constants obtained from the identification process.

3.6. Current-Dependent Bouc–Wen Model. Dominguez et al. [41] proposed a new Bouc–Wen model, in which the current is considered as a variable. In the standard Bouc–Wen model, the current is not considered a variable; therefore, the model parameters must be estimated for each current excitation. However, this can be computationally expensive. Upon entering the flow, (16) can be rewritten as follows:

$$F(x(\tau), \dot{x}(\tau), 0 \le \tau \le t, t) = c_0(I)\dot{x} + k_0(I)x + \alpha(I)z. \tag{28}$$

The evolutionary variable (z) is described by the following first-order differential equation:

$$\dot{z}(I) = \gamma(I)|\dot{x}|z|z|^{n-1} - \beta(I)\dot{x}|z|^n + A(I)\dot{x}. \tag{29}$$

If $A(I)$ and $\beta(I)$ are assumed to be unity and zero, respectively, $z(I)$ is obtained as follows:

$$\begin{aligned} z(I) &= \frac{1}{\sqrt{\gamma(I)}} \tanh\left\{\sqrt{\gamma(I)}\left[\dot{x} + \frac{1}{\sqrt{\gamma(I)}} \operatorname{arctanh}\left(\frac{F_{z0}(I)\sqrt{\gamma(I)}}{\alpha(I)}\right)\right]\right\} \text{ when } (z<0, x<0) \text{ or } (z\ge 0, x<0), \\ z(I) &= \frac{1}{\sqrt{\gamma(I)}} \tanh\left\{\sqrt{\gamma(I)}\left[\dot{x} + \frac{1}{\sqrt{\gamma(I)}} \operatorname{arctanh}\left(-\frac{F_{z0}(I)\sqrt{\gamma(I)}}{\alpha(I)}\right)\right]\right\} \text{ when } (z\ge 0, x\ge 0) \text{ or } (z<0, x\ge 0). \end{aligned} \tag{30}$$

In addition, owing to the experimental results, the relationship between the current and the parameters γ and k_0 is linear, and the parameters c_0, α, and F_{z0} change exponentially with the current.

$$\gamma(I) = -\gamma_1 + \gamma_2 I;\ k_0(I) = k_1 + k_2 I;\ c_0(I) = c_1 + c_2\left(1 - e^{-c_3 I}\right),$$
$$\alpha(I) = \alpha_1 + \alpha_2\left(1 - e^{-\alpha_3 I}\right);\ F_{z0}(I) = F_{z0_1} + F_{z0_2}\left(1 - e^{-F_{z0_3} I}\right). \tag{31}$$

3.7. Current-Frequency-Amplitude-Dependent Bouc–Wen Model. The model introduced in [41] for lower currents ($I = 0.25$ A) could not describe the damper behavior correctly; therefore, Dominguez et al. [42] proposed another model based on the Bouc–Wen model. In this model, the current, frequency, and excitation amplitude are incorporated as variables to determine the MR damper hysteresis behavior more accurately and effectively. Therefore, the Bouc–Wen model is modified as shown in the following equation:

$$F(x(\tau), \dot{x}(\tau), I, \omega, x, 0 \le \tau \le t; t) = \left(d_1 \omega^{d_2}\right)\left(d_3 x_{\max}^{d_4}\right)\left[c_0(I)\dot{x} + k_0(I)x + \alpha(I)z\right], \tag{32}$$

where ω is the excitation frequency; $x_{\max}$ is the excitation displacement amplitude; and $d_1, \ldots, d_4$ are constants. z is an evolutionary variable defined by the differential equation in (30). A linear relationship exists between the current and parameters γ and k_0. For the parameters c_0, α, and F_{z0}, this dependency is related to the values of the driven current. When the device current was low, these parameters changed linearly, and at the point of high current, an exponential relationship was chosen. A border value, I_c, was defined to separate the low and high current values. Dominguez et al. [65, 66] used this model in their study.

$$\gamma(I) = \gamma_1 - \gamma_2 I;\ k_0(I) = k_1 + k_2 I;\ c_0(I) = \begin{cases} c_1 + c_2\left(1 - e^{-c_3(I - I_c)}\right), & \text{for } I > I_c, \\ c_4 + \dfrac{(c_4 - c_1)}{I_c} I, & \text{for } I \le I_c, \end{cases}$$
$$\alpha(I) = \begin{cases} \alpha_1 + \alpha_2\left(1 - e^{-\alpha_3(I - I_c)}\right), & \text{for } I > I_c, \\ \alpha_4 + \dfrac{(\alpha_4 - \alpha_1)}{I_c} I, & \text{for } I \le I_c, \end{cases}; \quad F_{z0}(I) = \begin{cases} F_{z0_1} + F_{z0_2}\left(1 - e^{-F_{z0_3}(I - I_c)}\right), & \text{for } I > I_c, \\ F_{z0_4} + \dfrac{\left(F_{z0_4} - F_{z0_1}\right)}{I_c} I, & \text{for } I \le I_c. \end{cases} \tag{33}$$

3.8. Asymmetric Sigmoid Modified Bouc–Wen Model. Ma et al. [67] found that the Bouc–Wen model equation modified in [16] can be further modified. Spencer et al. [16] described the behavior of an MR damper linearly using current-dependent functions according to (20), whereas in the proposed model [67], the damper force can be described in a general form with two independent functions, as shown in the following equation:

$$f_d = f_i(i) f_h(x, \dot{x}, \ddot{x}), \tag{34}$$

where $f_i(i)$ represents the current function and $f_h(x, \dot{x}, \ddot{x})$ is a hysteresis function that can be the same as the modified Bouc–Wen model introduced by Spencer et al. [16] according to (17). The current function $f_i(i)$ is derived from the following equation

$$f_i(i) = 1 + \frac{k_2}{1 + e^{-a_2(i + I_0)}} - \frac{k_2}{1 + e^{-a_2 I_0}}, \quad i > 0, \tag{35}$$

where k_2 and a_2 are positive constants and I_0 is an arbitrary constant that represents a bias and is identified from experimental or benchmark data.

3.9. Nonsymmetrical Bouc–Wen Model. Because of nonsymmetrical hysteresis behavior that can be seen in the force-velocity response of some MR dampers, Kwok et al. [68] proposed a nonsymmetrical model based on the standard Bouc–Wen model. The evolutionary variable expressed in (15) can be rewritten as follows:

$$\dot{z} = \left[\delta - \left(\beta + \gamma \operatorname{sgn}(x)(z\dot{x})|z|^n\right]\dot{x}. \tag{36}$$

The nonsymmetrical Bouc–Wen model proposed by Kwok et al. [68] is obtained as (37) by adjusting the velocity value

$$\begin{aligned}(\dot{x} - \mu \operatorname{sgn}(x)) &\longrightarrow \dot{x},\\ \dot{z} &= \left[-\gamma \operatorname{sgn}\{[\dot{x} - \mu \operatorname{sgn}(x)]z\})|z|^n - \beta|z|^n + \delta\right][\dot{x} - \mu \operatorname{sgn}(x)],\end{aligned} \tag{37}$$

where μ is a scale factor for the adjustment and $\operatorname{sgn}(.)$ is a signum function. The force generated by the MR damper according to Figure 13 is obtained from the following equation:

$$F = c_0\dot{x} + k_0(x) + \alpha z, \tag{38}$$

where z is the asymmetric Bouc–Wen hysteresis operator expressed in (37). Note that the overall effect of the shift in the hysteresis switching is in the vicinity of zero velocity, whereas the form of hysteresis is maintained for the rest of the loop.

3.10. Normalized Bouc–Wen Model I. In the structural control literature, equations (37) and (38) are common forms of the general Bouc–Wen relations (equations (14), (15)).

$$\Phi_{\mathrm{BW}}(x,t) = \alpha k x(t) + (1-\alpha)\mathrm{Dkz}(t), \tag{39}$$

$$\dot{z} = D^{-1}\left(A\dot{x} - B|\dot{x}||z|^{n-1}z - \gamma\dot{x}|z|^n\right). \tag{40}$$

In this general form of the Bouc–Wen model, some parameters are redundant. To eliminate this redundancy, a normalized form of the Bouc–Wen model was proposed in [69–73] using a transition parameter $w(t)$:

$$w(t) = \frac{z(t)}{z_0};\ z_0 = \sqrt[n]{\frac{A}{\beta+\gamma}}. \tag{41}$$

Therefore, the Bouc–Wen model can be rewritten as

$$\Phi_{\mathrm{BW}}(x,t) = k_x x(t) + \kappa_w w(t), \tag{42}$$

$$\dot{w} = \rho\left(\dot{x} - \sigma|\dot{x}(t)||w(t)|^{n-1}w(t) + (\sigma-1)\dot{x}(t)|w(t)|^n\right), \tag{43}$$

where

$$\rho = \frac{A}{Dz_0} > 0;\ \sigma = \frac{\beta}{\beta+\gamma} \geq 0;\ \kappa_x = \alpha k > 0;\ \kappa_w = (1-\alpha)Dkz_0 > 0. \tag{44}$$

The normalized form of the Bouc–Wen model is an equivalent representation of the original Bouc–Wen model. This model has fewer parameters; therefore, the over-parameterization in the original Bouc–Wen model was removed. In this representation, the evolutionary variable is in the range [−1, 1] [59].

Tsouroukdissian et al. [74] proposed a normalized Bouc–Wen model for small-scale MR dampers. Their proposed model have the same form as (42), with one major difference: they replace x with $\dot{x}$. Therefore, the force generated by the MR damper is obtained from the following equation:

$$F(t) = k_x\dot{x}(t) - k_w w(t). \tag{45}$$

Parameter $w(t)$ is calculated using (43). Equation (45) is more compatible with the force-velocity behavior of MR dampers. Parameters k_x, σ, and n are constant values, and k_w is considered a linear variable with voltage. In their research, two different forms were considered for ρ: a linear voltage-dependent relation or a constant value. The results showed that the accuracy of the first model (voltage-dependent) was higher than that of the second. In 2009, Rodriguez et al. [75] used the same normalized Bouc–Wen model [47] for a large-scale MR damper.

Bahar et al. [76] modified the normalized Bouc–Wen model for a large-scale MR damper. To improve the model accuracy for large-scale dampers, they developed normalized Bouc–Wen model parameters, as shown in the following equation:

$$F(t) = k_x x(t) + k_{\dot{x}}\dot{x}(t) - k_w w(t). \tag{46}$$

The first term in this formula, $k_x x(t)$, represents the linear-elastic force added to (45). According to the parameter identification results, k_x is constant and $k_{\dot{x}}$ changes

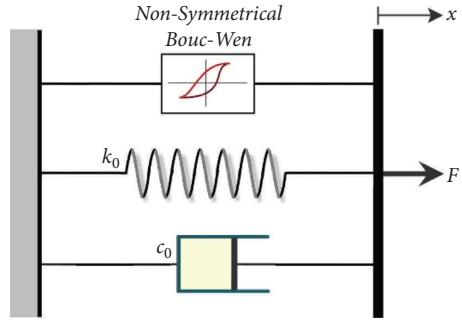

Figure 13: Nonsymmetrical Bouc–Wen model (Section 3.9).

linearly with voltage. The parameters n, ρ, and σ change exponentially. The identified k_w has a more complicated relationship with the voltage.

$$k_{\dot{x}}(v) = k_{\dot{x}a} + k_{\dot{x}b}v;\ n(v) = n_a + n_b \exp(-13v);$$
$$\rho(v) = \rho_a + \rho_b \exp(-14v);\ \sigma(v) = \sigma_a + \sigma_b \exp(-14v), \tag{47}$$

$$k_w(v) = \begin{cases} k_{w1} + k_{w2}v^{1.13}, & v \le 0.3, \\ k_{w3} + k_{w4}\sin\left(\dfrac{\pi(v-0.3)}{0.8}\right) + k_{w5}\sin\left(\dfrac{3\pi(v-0.3)}{0.8}\right), & 0.3 \le v \le 0.7, \\ k_{w6} + k_{w7}v + k_{w8}v^3 + k_{w9}v^5, & 0.7 \le v. \end{cases} \tag{48}$$

In 2010, the same group [77] used their model as an MR damper in a benchmark structure and proposed a new successful hierarchical control algorithm.

3.11. Normalized Bouc–Wen Model II. The model proposed by Dominguez et al. [42] has several parameters. This redundancy makes the identification and modeling procedure of the MR damper complex. Dominguez et al. [43], based on the same models [41, 42], presented a new model with fewer parameters and higher accuracy. If in (29), β is zero, then n is assumed to be equal to z and $A = \gamma$. The evolutionary variable (z) becomes normalized and has the simple form of the following equation:

$$\dot{z} = -\gamma|\dot{x}||\dot{x}|^{z-1}z + \gamma\dot{x} = \gamma(\dot{x} - |\dot{x}||z|z). \tag{49}$$

Parameter z was obtained from the solution of the above equation.

$$z = \tanh(\gamma(x + \lambda_i));\ i = 1.2\begin{cases} z \ge 0,\ \dot{x} \ge 0, \\ z < 0,\ \dot{x} < 0, \end{cases} i = 3.4\begin{cases} z \ge 0, \dot{x} < 0, \\ z < 0, \dot{x} \ge 0. \end{cases} \tag{50}$$

In the above equation, λ_i is a constant originating from integration. As the MR damper hysteresis force is velocity-dependent in practice, in (49), the velocity is replaced by the displacement (i.e., $\dot{x}$ is replaced by x), as shown in the following equation:

$$z = \tanh(\gamma(x + \lambda_0))\begin{cases} z \ge 0,\ \dot{x} \ge 0, \\ z < 0,\ \dot{x} < 0, \end{cases} z = \tanh(\gamma(x + \lambda_1))\begin{cases} z \ge 0, \dot{x} < 0, \\ z < 0, \dot{x} \ge 0. \end{cases} \tag{51}$$

The first part of (51) shows the upper curve of the hysteresis loop and the second part shows the lower curve. The force generated by a damper in such a model is expressed as follows:

$$F(x(\tau), \dot{x}(\tau), 0 \le \tau \le t;\ t) = k_0 x + c_0 \dot{x} + \rho z. \tag{52}$$

The parameter ρ is a new evolutionary parameter. It is used instead of the parameter α in the previous form of the Bouc–Wen model presented in (22). The parameters ρ, c_0, and k_0 can be approximated by the root-squared function weighted by the proper constants. Parameter λ did not change significantly with respect to the current variation. Therefore, it can be considered a constant parameter.

$$\begin{aligned} c_0(I) &= c_1 + c_2\sqrt{|I|};\ k_0(I) = k_1 + k_2\sqrt{|I|};\ \rho(I, \dot{x}) \\ &= \rho_1 + \rho_2\sqrt{|I|} + \rho_3\sqrt{|\dot{x}|}. \end{aligned} \tag{53}$$

Another effectual decrease is that Dominguez et al. [65] assumed that the integration constant parameter λ could be approximated by $-\ddot{x}$. With this change, (49) is written as the following equation:

$$z = \tanh(\gamma(\dot{x} - \ddot{x})). \tag{54}$$

While the Bouc–Wen model is widely used, it exhibits two primary shortcomings when characterizing the hysteresis phenomenon. First, there is a significant discrepancy between the hysteresis curves derived from experimental data and the model when assessing constant characteristic parameters. Optimizing these parameters demands substantial computational effort. Second, the model's performance hinges on specific excitation conditions. Typically, the hysteresis loop is formulated for a harmonic excitation characterized by a defined amplitude, frequency, and current excitation. Altering these conditions necessitates recalibrating the Bouc–Wen parameters. Recognizing these challenges, Dominguez et al. [43] introduced a normalized Bouc–Wen model that streamlines the number of constant characteristic parameters. They elucidated the impact of each parameter on the hysteresis loop and proposed an innovative method to extract these parameters from experimental data. Conclusively, they presented a model rooted in the normalized Bouc–Wen framework, wherein displacement, velocity, acceleration, and current excitation serve as inputs, with the hysteresis force as the output.

3.12. Normalized Phenomenological Model. Bai et al. [78] introduced a normalized phenomenological model by incorporating the concept of normalization into the modified Bouc–Wen model. In the modified Bouc–Wen model or phenomenological models shown in Figure 8, a dashpot denoted by c_1 is connected in series with the Bouc–Wen model to generate the roll-off force at low velocities. Such combinations increase the capacity of the model to describe the hysteresis behavior of the MR damper. However, the complexity of the model also increases because of the differential equation required to represent the dashpot. The concept of normalizing the Bouc–Wen model was introduced by Ikhouane and Rodellar [70–72], as discussed in the previous section. By incorporating the normalized Bouc–Wen model into the phenomenological model, (17) can be written as

$$\dot{z} = \rho\left(-\sigma|\dot{x} - \dot{y}|z|z|^{n-1} - (1-\sigma)(\dot{x} - \dot{y})|z|^n + (\dot{x} - \dot{y})\right). \tag{55}$$

The above equation, when replaced with a similar relation as in (17), initiates the normalized phenomenological model.

The intricacy of the phenomenological model somewhat restricts its applicability in real-time control systems. To address this, researchers simplified the model, focusing on both its structural and expressive facets. One particular challenge is the inclusion of the dashpot in the phenomenological model. Its presence augments the complexity of the mathematical model, primarily due to the differential equation that describes the dashpot, complicating the parameter identification process. However, by incorporating the concept of normalization within the phenomenological model, it is possible to decrease the number of parameters by one.

3.13. Restructured Model. Figure 14 shows a schematic of the restructured model proposed by Bai et al. [78]. The restructured model was inspired by the phenomenological or modified Bouc–Wen model [16]. They removed the elastic element, k_0, of the phenomenological model. The position of segment c_0 moves and is located parallel to the springy component, k_0. By incorporating the normalization concept, the restructured model can be written as follows:

$$\begin{aligned} &F = k_1 x + c_0 \dot{x} + \alpha z + f_0, \\ &\dot{y} = \frac{\alpha z}{c_1};\ \dot{z} = \rho\left(-|\dot{x} - \dot{y}|z|z|^{n-1} - (1-\sigma)(\dot{x} - \dot{y})|z|^n + (\dot{x} - \dot{y})\right). \end{aligned} \tag{56}$$

The use of the restructured model is more straightforward than the modified Bouc–Wen model [16] because of the lower dependency between the parameters. Through the modification of the phenomenological model's structure and the integration of the normalization concept, a restructured model was introduced. This new model boasts a more streamlined and lucid structure, facilitating computer simulations and the parameter identification process. As a result, the foundational structure of the restructured model is an evolution from the original phenomenological model, with the added benefit of a reduced parameter count.

4. LuGre Models

Canudas et al. [79] proposed a dynamic model for friction that captures most of the experimentally observed friction behavior. This includes the Stribeck effect, hysteresis, spring-like characteristics for stiction, and varying breakaway forces. The model has the following form and is characterized by parameters a_0, σ_0, σ_1, and σ_2.

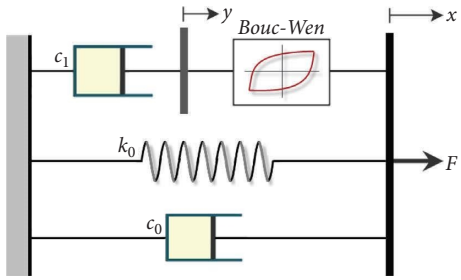

Figure 14: Restructured model (Section 3.13).

$$F = \sigma_0 z + \sigma_1 \dot{z} + \sigma_2 \dot{x},\ \dot{z} = \dot{x} - \sigma_0 a_0 |\dot{x}| z. \tag{57}$$

Traditional models fall short in capturing the hysteretic behavior observed during the study of friction at transient velocities. Additionally, they fail to account for variations in the breakaway force based on experimental conditions and the minor displacements in the contact region during stiction. Addressing these gaps, Canudas et al. [79] introduced a dynamic friction model that melds the Dahl effect, representing stiction behavior, with arbitrary steady-state friction properties, potentially encompassing the Stribeck effect.

In 2002, Alvarez and Jiménez [80] modified this model by considering the effect of the magnetic field and assumed that the current that determines the intensity of the field is proportional to the applied voltage. The modified model is

$$F = \sigma_0 z v + \sigma_1 \dot{z} + \sigma_2 \dot{x},\ \dot{z} = \dot{x} - \sigma_0 a_0 |\dot{x}| z \left(1 + a_1 v\right). \tag{58}$$

The novel modeling approach, grounded in the first-order dynamic friction model of LuGre for MR dampers, boasts a more streamlined analytical structure. Impressively, it retains the capability to replicate force responses across various excitation signal types. A salient characteristic of this modeling framework is its facilitation of real-time parametric identification for the MR damper model parameters. This is possible because, with suitable parameter manipulation, the model can be linearized [80].

Sakai et al. [81] proposed a modified model to produce a simple model which can create an inverse model and express the dynamic friction characteristics, as well as the hysteresis effect. The modified model is described as

$$F = \sigma_0 z v + \sigma_1 \dot{z} + \sigma_2 \dot{x} + \sigma_a z + \sigma_b \dot{x} v,\ \dot{z} = \dot{x} - \sigma_0 a_0 |\dot{x}| z \left(1 + a_1 v\right). \tag{59}$$

Sakai et al. [81] aimed to introduce a model capable of predicting the damping force using the MR damper's velocity, internal state, and input voltage. Beyond this primary capability, their proposed model can also generate an inverse dynamic model, thereby determining the necessary input voltage from a given desired damping force. This advancement was motivated by the limitations of the model presented by Canudas et al. [79], which, despite its fewer parameters and capacity to articulate the hysteresis function, fell short in efficiently computing the optimal input voltage.

To manage the MR damper during the control process, Palka et al. [82] proposed an inversion of the LuGre model with thirteen parameters.

5. Biviscous Models

Biviscous models are another group of relations used to describe the nonlinear behavior of magnetorheological dampers. Generally, they are presented as piecewise lines or curves in a force-velocity diagram to illustrate the hysteresis behavior of MR dampers.

5.1. Nonlinear Biviscous Model. Instead of assuming that the materials are rigid in preyield circumstances, Stanway et al. [83] assumed that the materials in both the preyield and postyield states behave plastically. Based on this assumption, Wereley et al. [31], Pang et al. [32], and Snyder et al. [33] have proposed nonlinear biviscous models. They assumed that the preyield damping C_{pre} was much larger than the postyield damping C_{post} ($C_{\text{pre}} > C_{\text{post}}$). Therefore, the yield force can be determined by an extension of the postyield force line on the force-velocity curve and its intersection with the force axis, as shown in Figure 15. The force generated by this model is expressed as follows:

$$F(t) = \begin{cases} C_{\text{post}} + F_y & \dot{x} \geq \dot{x}_y, \\ C_{\text{pre}} \dot{x} & -\dot{x}_y \leq \dot{x} \leq \dot{x}_y,\ \dot{x}_y = \dfrac{F_y}{C_{\text{pre}} - C_{\text{post}}}, \\ C_{\text{post}} - F_y & -\dot{x}_y \geq \dot{x}, \end{cases} \tag{60}$$

where $\dot{x}_y$ denotes the yield velocity.

5.2. Nonlinear Hysteretic Biviscous Model. This model was proposed by Wereley et al. [31] in 1998, based on observations during experiments. As shown in Figure 16, the nonlinear hysteretic biviscous model [31–33, 84, 85] comprises four main parts. The resultant force-velocity diagram of the damper shows a distinct preyield hysteresis phenomenon. The nonlinear hysteresis biviscous model is an extension of the nonlinear biviscous model described in the previous section. Extension in the preyield region was achieved by adding a new parameter. This new parameter is at the intersection of the zero-force line with the force-velocity curve, which is termed $\dot{x}_0$. Equation (61) generates the damping force of this model. In this equation, $\dot{x}_{y1}$ is the decelerating yield velocity and $\dot{x}_{y2}$ is the accelerating yield velocity.

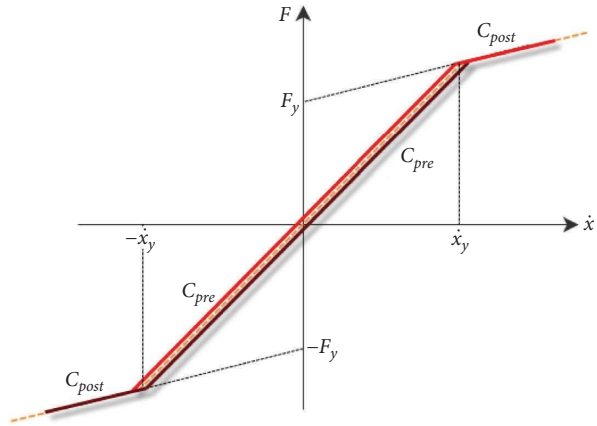

Figure 15: Nonlinear biviscous model (Section 5.1).

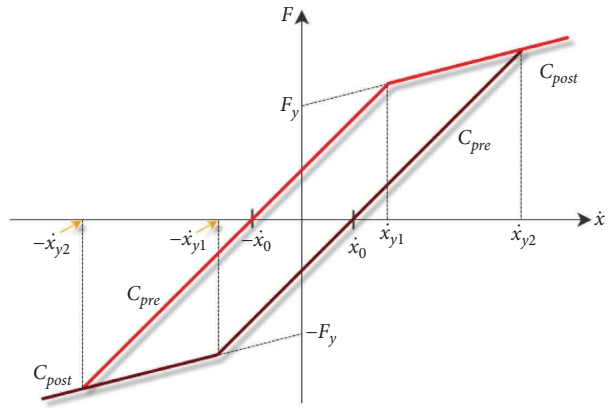

Figure 16: Nonlinear hysteretic biviscous model (Section 5.2).

$$F(t) = \begin{cases} C_{\text{post}}\dot{x} - F_y, & \dot{x} \le \dot{x}_{y1};\ \ddot{x} > 0, \\ C_{\text{pre}}(\dot{x} - \dot{x}_0), & -\dot{x}_{y1} \le \dot{x} \le -\dot{x}_{y2};\ \ddot{x} > 0, \\ C_{\text{post}}\dot{x} + F_y, & \dot{x}_{y2} \le \dot{x};\ \ddot{x} > 0, \\ C_{\text{post}}\dot{x} + F_y, & \dot{x}_{y1} \le \dot{x};\ \ddot{x} < 0, \\ C_{\text{pre}}(\dot{x} + \dot{x}_0), & -\dot{x}_{y2} \le \dot{x} \le -\dot{x}_{y1};\ \ddot{x} < 0, \\ C_{\text{post}}\dot{x} - F_y, & \dot{x} \le -\dot{x}_{y2};\ \ddot{x} < 0, \end{cases} \quad \dot{x}_{y1} = \frac{F_y - C_{\text{pre}}\dot{x}_0}{C_{\text{pre}} - C_{\text{post}}};\ \dot{x}_{y2} = \frac{F_y + C_{\text{pre}}\dot{x}_0}{C_{\text{pre}} - C_{\text{post}}}. \tag{61}$$

Wereley et al. [31] suggested some current-dependent relations for the four main parameters of their model: C_{pre}, C_{post}, $\dot{x}_0$, and F_y. Based on the results obtained from the experimental data, second-order polynomials are needed for C_{pre}, C_{post}, and F_y, whereas fourth-order polynomials are required for $\dot{x}_0$ as functions of the applied current.

5.3. Nonlinear Hysteretic Arctangent Model. Wang and Liao [86] introduced a model from Ang et al. [87] that describes the force-velocity relation of the hysteresis loop according to the following equation:

$$F(t) = \begin{cases} C_{\text{post}}\dot{x} - F_{y,} & \dot{x} \le \dot{x}_{y1};\ \ddot{x} > 0, \\ \alpha \arctan[\beta(\dot{x} - \dot{x}_0)], & -\dot{x}_{y1} \le \dot{x} \le -\dot{x}_{y2};\ \ddot{x} > 0, \\ C_{\text{post}}\dot{x} + F_y, & \dot{x}_{y2} \le \dot{x};\ \ddot{x} > 0, \\ C_{\text{post}}\dot{x} + F_y, & \dot{x}_{y1} \le \dot{x};\ \ddot{x} < 0, \\ \alpha \arctan[\beta(\dot{x} + \dot{x}_0)], & -\dot{x}_{y2} \le \dot{x} \le -\dot{x}_{y1};\ \ddot{x} < 0, \\ C_{\text{post}}\dot{x} - F_y, & \dot{x} \le -\dot{x}_{y2};\ \ddot{x} < 0. \end{cases} \tag{62}$$

In (62), α is the magnification factor and β is the rotation factor. These parameters must be detected from the shape of the resulting force-velocity curve. The proposed model

produces a symmetric hysteresis loop around the zero point of the coordinate system.

5.4. Lumped-Parameter Model of Fluid Flow. Sims et al. [88] introduced a lumped-parameter model for fluid flow within MR dampers. Their design conceptualizes fluid motion through a lumped-parameter model intrinsically tied to the device's geometry, as depicted in Figure 17. They contended that such models should not only predict the damper's performance in isolation but also its behavior within a more intricate vibrating structure. This perspective diverged from earlier modeling priorities, which predominantly emphasized the damper's standalone performance, often characterized under sinusoidal excitation and open-loop scenarios. In response to these evolving needs, the authors advanced a modeling technique that balances these distinct prerequisites while retaining the paramount physical relevance of core parameters. Additionally, their approach facilitates system identification or model revision, ensuring that the model faithfully mirrors observed behaviors. Figure 18 shows a schematic representation of the model with lumped parameters. The equations of motion for this object are as follows:

$$(a)\, k(x_2 - x_1) - \psi(\dot{x}_1 .H) = m_1 \ddot{x}_1 \; ; \; (b)\, F - k(x_2 - x_1) = m_2 \ddot{x}_2 . \tag{63}$$

Here, the quasisteady valve flow is represented by a nonlinear ψ function, which is a function of the quasisteady velocity x_1 and management signal H. For an MR damper, this signal is typically an electrical current (I) that generates a magnetic field in the valve. Fluid compressibility is indicated by a spring with stiffness k. Fluid inertia is denoted by m_1. F is the force applied to the damper, which causes piston movement (x_2). An additional mass (m_2) is used to consider the mass of the piston parts and accessories. The physical significance of the model is its ability to define its parameters based on constitutive relationships using fluid properties and device. It is not necessary to observe the behavior of the actual appliance. This implies that the model can be developed before the device is built; thus, it is a suitable tool for the prototype design of a damper.

The quasisteady behavior described by ψ can be described in a biviscous function format that follows:

$$\psi(\dot{x}_1 , I) = \begin{cases} C_{\text{pre}} \dot{x}, & \dot{x} \le \dfrac{F_y}{C_{\text{pre}}}, \\ C_{\text{post}} \dot{x} + F_y \operatorname{sgn}(\dot{x}), & \dot{x} > \dfrac{F_y}{C_{\text{pre}}}. \end{cases} \tag{64}$$

The relationship between C_{pre}, C_{post}, and F_y with the current applied to the damper (I) can be expressed as (65) using the hyperbolic tangent function.

$$C_{\text{pre}}(I) = C_{\text{pre}_a} + C_{\text{pre}_b} \tanh\left(C_{\text{pre}_c} I\right); \; C_{\text{post}}(I) = C_{\text{post}_a} + C_{\text{post}_b} \tanh\left(C_{\text{post}_c} I\right); \; F_y(I) = F_{Y_a} + F_{Y_b} \tanh\left(F_{Y_c} I\right). \tag{65}$$

6. Viscoelastic-Plastic Models

Weiss et al. [89] and Jolly et al. [90] indicated that MR fluid behaves as a viscoelastic fluid in the preyield region and as a viscoplastic fluid in the postyield region. Based on this knowledge and perception, some viscoelastic-plastic models have been developed.

6.1. Nonlinear Viscoelastic-Plastic Model. Kammat and Wereley [91, 92] pioneered the introduction of a nonlinear viscoelastic-plastic model tailored for electrorheological (ER) dampers, bridging the input of shear strain with the resultant shear stress response. This model ingeniously amalgamates linear shear flow mechanisms in a nonlinear manner to characterize the ER fluid behavior across a spectrum of electric field strengths. By utilizing a minimal set of parameters coupled with straightforward linear mechanisms, the model adeptly captures the intricate dynamics of ER fluids. Furthermore, it obviates the need to grapple with computationally challenging nonlinear mechanisms, such as those represented by the Coulomb friction model. Subsequently, it extended it to the MR dampers [32, 33]. Based on the force-velocity hysteresis loop of the MR dampers, there are two distinct rheological regions: the preyield and postyield regions. The preyield area demonstrates strong hysteresis, which is regular for the viscoelastic behavior of such materials. The postyield region changes with a nonzero yield force, in which the yield force is a function of the applied current (e.g., changes in the magnetic field). The structure of the nonlinear viscoelastic-plastic model introduced by Pang et al. [32] is based on the block diagram in Figure 19.

6.1.1. Preyield Mechanism. The Kelvin element in Figure 20(a) represents the mechanical analogy of the viscoelastic damper's behavior in the preyield region. Equation (66) expresses this mechanism in the time domain.

$$F_{ve} = c_{ve} \dot{x}(t) + k_{ve} x(t), \tag{66}$$

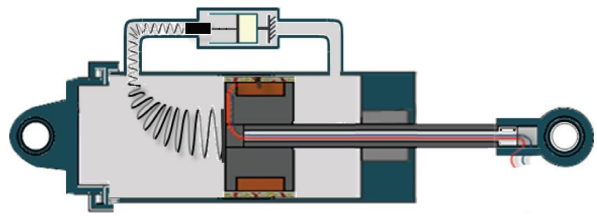

Figure 17: Schematic lumped-parameter representation of fluid flow (Section 5.4).

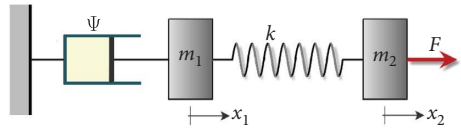

Figure 18: Lumped model of fluid flow (Section 5.4).

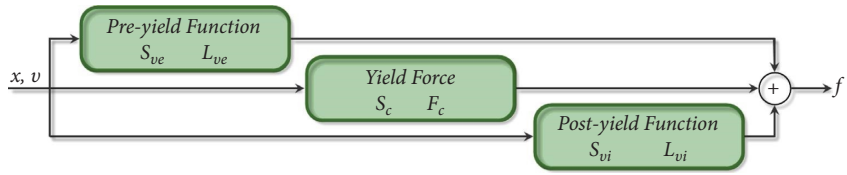

Figure 19: Overall structure of the nonlinear viscoelastic-plastic model (Section 6.1).

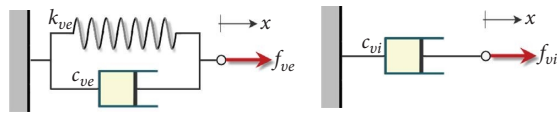

Figure 20: Overall structure of the model (Section 6.1).

where F_{ve} is the viscoelastic element of the damper force. The nonlinear shape function S_{ve} is a preyield switching function. This is parallel to the postyield switching function. S_{vi} undergoes a smooth transition from the preyield to postyield phase. The S_{ve} function depends on the yield velocity (v_g) and is established during the identification process. S_{ve} is obtained from the following equation:

$$S_{ve} = \frac{1}{2}\left[1 - \tanh\left(\frac{|v| - v_y}{4\varepsilon_y}\right)\right]. \tag{67}$$

In the above equation, $v(t)$ is the instantaneous velocity, v_y is the yield velocity, and ε_y is a smoothing parameter. The force component is obtained as a derivative of the preyield mechanism.

$$F_{\text{pre}}(t) = S_{ve}(v)F_{ve}(t). \tag{68}$$

6.1.2. Postyield Mechanism. In the postyield stage, the damper behavior is similar to a viscous damping device with a nonzero yield force. The postyield mechanical simulation, F_{vi}, is shown in Figure 20(b) as a viscous element. The force is expressed as follows:

$$F_{vi}(t) = c_{vi}v(t), \tag{69}$$

where S_{vi} is a shape function similar to S_{ve}. This function fulfills as a switching operation to trigger a postyield viscous mechanism when the damping force exceeds the yield force. This is obtained using the following equation:

$$S_{vi} = \frac{1}{2}\left[1 + \tanh\left(\frac{|v| - v_y}{4\varepsilon_y}\right)\right]. \tag{70}$$

Therefore, the force component of the postyield mechanism is as follows:

$$F_{\text{post}}(t) = S_{vi}(v)F_{vi}(t). \tag{71}$$

6.1.3. Yield Force. The yield force F_c is a function of the applied domain and is a domain-dependent parameter that provides the damper with its semiactive capabilities. The damper behavior shows some forms of the Coulomb force effect at low velocity. This effect is included in the force parameter F_c and the shape function S_c. The shape function is given by the following equation:

$$S_v = \frac{1}{2}\left[1 + \tanh\left(\frac{v}{4\varepsilon_y}\right)\right]. \tag{72}$$

In the above equation, $v(t)$ is the velocity magnitude and v_c is a smoothing factor that ensures a smooth transition from a negative velocity to a positive value and vice versa.

$$F_c(t) = S_c(v)F_c. \tag{73}$$

6.1.4. Final Form of the Viscoelastic-Plastic Model. Equation (74) shows the final form of the damping force of the viscoelastic-plastic model.

$$\begin{aligned} F(t) &= F_{\text{pre}}(t) + F_{\text{post}}(t) + F_c(t) \\ &= S_{ve}(v)F_{ve} + S_{vi}(v)F_{vi} + S_c(v)F_c. \end{aligned} \tag{74}$$

The assumption behind this equation is that the damping force is a combination of functions, each of which is a linear mechanism with nonlinear shape functions.

6.2. Viscoelastic-Plastic Model Proposed by Wereley. In 1980, Wereley et al. [93, 94] used the previously described preyield and postyield mechanisms and proposed a viscoelastic-plastic model by changing the transition function from the preyield to the postyield regions. The researchers observed that prevailing dynamic models heavily lean on experimental data. While this reliance is somewhat inescapable given the intricate material behaviors at play, the absence of a phenomenological approach in modeling ER fluid often amplifies the volume of experimental data needed for parameter estimation. Notably, models of this nature typically encompass a limited set of parameters. As a solution, they introduced a nonlinear viscoelastic-plastic model, embodying a novel approach to characterize ER fluid. A schematic representation of this model can be seen in Figure 21.

As shown in Figure 21, in this viscoelastic-plastic model and unlike in Figure 19, there is no yield force, and its descriptive relation is given by the following equation:

$$\widehat{F}_{\text{MR}_{\text{effective}}} = S_{ve}F_{ve} + S_{vi}F_{vi}, \tag{75}$$

where S_{ve} and S_{vi} are the nonlinear preyield and postyield shape functions, respectively, obtained from equations (69) and (65). F_{ve} and F_{vi} are the pre and postyield damping force components obtained from equations (61) and (64), respectively.

6.3. Viscoelastic-Plastic Model Proposed by Li. Li et al. [20] started using a mechanism similar to that of the viscoelastic-plastic modeling introduced by Wereley et al. [93, 94] to model the behavior of the MR damper, whereafter they modified the preyield and postyield mechanisms of the viscoelastic-plastic model. As shown in Figure 22, they developed a new model for the MR damper by integrating a rigid three-parameter model, similar to the mechanism used for viscoelastic behavior in the preyield region (Figure 22(a)). This model consists of a spring (k_2) connected in series with a rigid Kelvin–Voigt model, represented by k_1 and c_1.

In addition to the viscoelastic force F_{ve}, the stiction effect (F_s) resulting from the piston seal enters the damping force. Therefore, the damping force in the preyield region is given by the following equation:

$$F = F_{ve} + F_S. \tag{76}$$

When the damper force F is higher than the yield force of the damper F_c, the MR damper operates in the postyield phase. Both the inertial components and the fluid viscous residence contributed to the yield force. Therefore, the damper's postyield force (F_p) can be expressed as follows:

$$F_p = F_c \operatorname{sgn}(\dot{x}) + c_v\dot{x} + R\ddot{x}. \tag{77}$$

In (77), c_v is the viscous coefficient and R is the equivalent inertial mass. By combining these two phases, the resulting equation for the model proposed by Li et al. [20] was obtained as follows:

$$F = F_{ve} + F_S,\ |F| \le F_c, \tag{78}$$

$$F_p = F_c \operatorname{sgn}(\dot{x}) + c_v\dot{x} + R\ddot{x},\ |F| > F_c. \tag{79}$$

6.4. Viscoelastic-Plastic Continuous Physical Model (VEP). To design an intelligent suspension system for high-speed trains, Li et al. [95] sought an accurate model of the MR damper. The optimal model was envisaged to fulfill three core criteria: (1) accurately capture the intrinsic nonlinear behavior of the damper; (2) ensure that the model parameters carry tangible physical interpretations; and (3) establish a direct linkage between model parameters and the MR damper's performance. However, the model proposed by Wereley et al. [93, 94] demonstrated constraints in representing the dynamic hysteresis loop during variable frequency excitations. Addressing this, Li et al. proposed a viscoelastic-plastic model, determining its operational boundaries by assessing whether the prey-ielding force surpasses the yielding threshold. This model, termed the continuous viscoelastic-plastic physical model, is anchored in a comprehensive exploration of a damper's functional mechanisms and an analysis of its dynamic behavior. This article delves into the development journey of this model. Notably, the Maxwell model serves as a common mechanical counterpart for understanding viscoelastic phenomena in the prestrain phase, as depicted in Figure 23. Equation (80) shows the resulting equations for this model.

$$F_{\text{pre}} = c_{\text{pre}}\dot{y} = kx - y, \tag{80}$$

where k is the stiffness and C_{pre} is the viscous damping coefficient of the preyield phase. The viscous-plastic behavior in the postyield phase was described using the Bingham model (Figure 24). The damping force in the postyield region is expressed as follows:

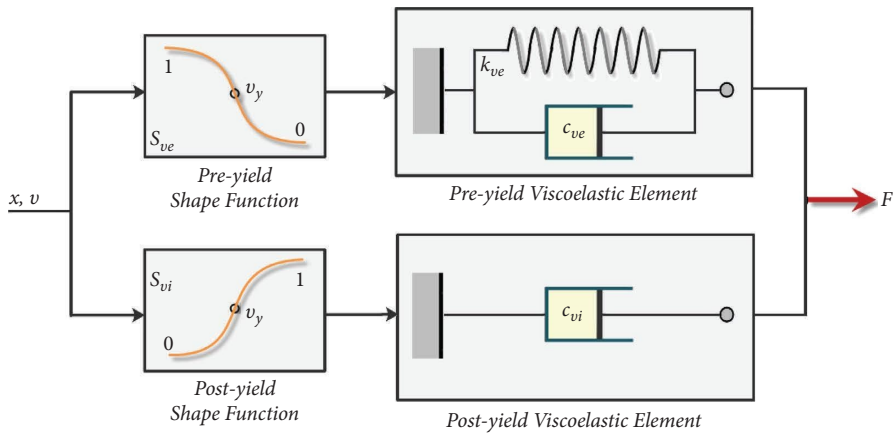

Figure 21: Overall structure of the viscoelastic-plastic model by Wereley et al. [93, 94] (Section 6.2).

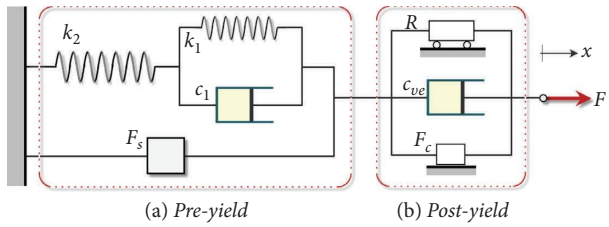

Figure 22: Overall structure of the model proposed by Li et al. [20] (Section 6.3).

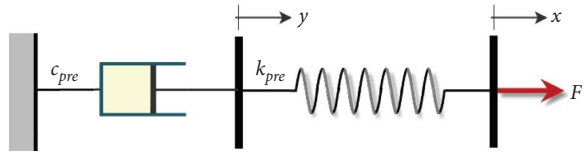

Figure 23: Mechanical analogy of the viscoelastic phenomena in the preyield phase (Section 6.4).

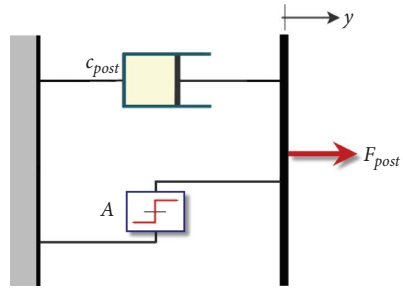

Figure 24: Viscous plastic model in preyield phase (Section 6.4).

$$F_{\text{post}} = C_{\text{post}}\dot{y} + A\,\text{sgn}(\dot{y}), \tag{81}$$

where A is the yield force and C_{post} is the viscous damping coefficient in the postyield region. Li et al. [95] used a new hyperbolic function to describe the transition path from the preyield to the postyield regions, as shown in Figure 25. A smooth curve of the yielding process can be obtained by merging $C_{\text{pre}}\dot{y}$ and $A\,\text{sgn}(\dot{y})$ as a new function. Thus, both the Maxwell and Bingham models were merged into the viscoelastic-plastic model, as shown in Figure 26. The final equation can be rewritten as follows:

$$F = kx - y = c\dot{y} + A \quad \tanh(\alpha\dot{y}), \tag{82}$$

where F denotes the damping force of the damper, k denotes the stiffness of the damper in the preyield region, c denotes the viscous damping coefficient in the postyield region, A denotes the yield force, and α denotes the restoring factor.

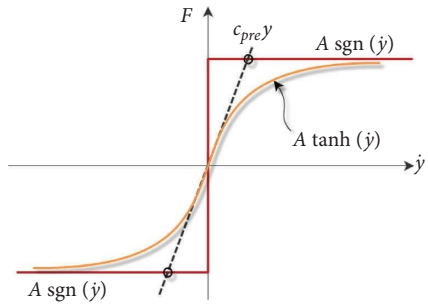

Figure 25: Transition function from preyield to postyield region (Section 6.4).

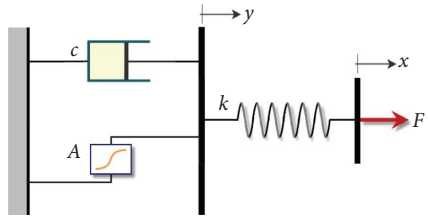

Figure 26: Viscoelastic-plastic continuous physical model (Section 6.4).

6.5. Nonlinear Stiffness Viscoelastic-Plastic Model (nkVEP). Li et al. [95] observed a sudden decline in the slope of the force-displacement and force-velocity curves derived from MR damper behavior, particularly within the preyield region. This abrupt deviation is largely attributable to the damper's inadequate internal pressure. While bolstering the pressure in the reservoir can mitigate this effect, it cannot be entirely eradicated. Earlier viscoelastic-plastic models fell short in capturing this distinct decline in force-velocity and force-displacement relationships. Consequently, there was a palpable need to formulate a model that aptly represents this phenomenon. Based on this finding, they proposed a viscoelastic-plastic model with nonlinear stiffness (nkVEP), as shown in Figure 27. The equation for this model is in the form of the following equation:

$$F = k(x, y)(x - y) = c\dot{y} + A \quad \tanh(\alpha\dot{y}). \tag{83}$$

By fitting the nonlinear stiffness data, the function $k(x, y)$ can be rewritten as

$$k(x, y) = q\left|(x - y) - \tanh\left(\rho(\dot{x} - \dot{y})d_{\text{opf}}\right)\right|^{n} + k_0, \tag{84}$$

where ρ is the amplification coefficient, d_{opf} is the position of the sudden change point in the stiffness, and k_0 is the reference value of the stiffness. In addition, the main parameters of the nkVEP model were presented for the generalized fluctuating current (i) according to the following equations:

$$A = A_a i + A_b;\ c = c_a i + c_b;\ k = k_a \tanh(bi) + k_b;\ \alpha = \alpha_a i + \alpha_b. \tag{85}$$

6.6. Stiffness-Viscosity-Elasto-Slide (SVES) Models. The nonlinear SVES model includes a linear combination of nonlinear mechanisms. Figure 28 shows a schematic of the SVES model proposed by Wereley et al. [93] to describe the hysteresis behavior of the MR dampers. Their model has three parallel amplitude-dependent elements: linear stiffness, linear viscous dashpot, and a nonlinear elasto-slide element consisting of a stiffness and Coulomb element in series. Figure 29 shows the effects of each of these mechanisms on the hysteresis loop of the damper. The linear stiffness and dashpot parameters provide the necessary slope and damping characteristics for the hysteresis loop. The elasto-slide element conveys stiffness in the region where the velocity of the damper changes its sign, and the displacement from the extreme position is less than a specific value ($2x_s$). The elasto-slide element is equivalent to a Coulomb element for the memory phenomenon of the hysteresis loop.

The force predicted by this model is

$$F(t) = F_s(t) + F_d(t) + F_{es}(t), \tag{86}$$

where $F_s(t)$ is the stiffness element force, $F_c(t)$ is the viscous dashpot element force, and $F_{es}(t)$ is the elasto-slide element force (four legs as a parallelogram), as shown in the following equation:

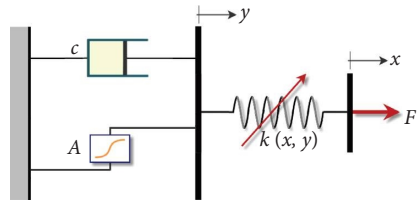

Figure 27: Nonlinear stiffness viscoelastic-plastic model (Section 6.5).

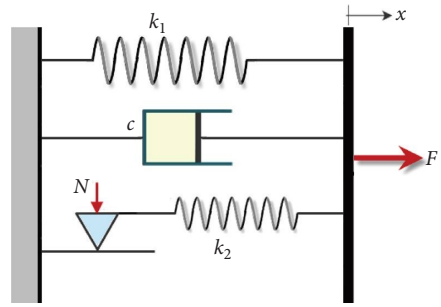

Figure 28: SVES models (Section 6.6).

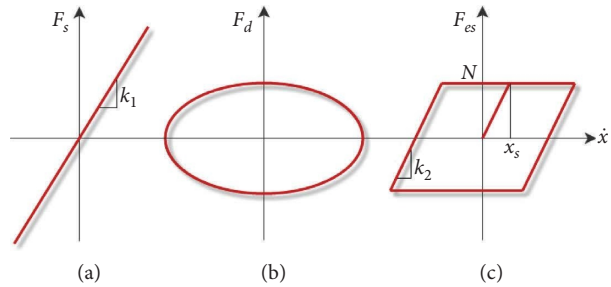

Figure 29: Elements of the hysteresis loop. (a) Linear stiffness element, (b) linear viscous damping element, and (c) nonlinear elasto-slide element (Section 6.6).

$$F_s(t) = k_1 x;\ F_d(t) = c\dot{x};\ F_{es}(t) = \begin{cases} -N, & x = \dot{x} \quad \dot{x} = 0, \\ -N + k_2(x + \overline{x}), & x < -\overline{x} + 2x_s \quad \dot{x} > 0, \\ N, & x > -\overline{x} + 2x_s \quad \dot{x} > 0, \\ N, & x = \dot{x} \quad \dot{x} = 0, \\ -N + k_2(x - \overline{x}), & x > -\overline{x} - 2x_s \quad \dot{x} < 0, \\ -N, & x < \overline{x} - 2x_s \quad \dot{x} < 0. \end{cases} \tag{87}$$

In (87), the sliding force (N) is given by the yielding displacement (x_s) multiplied by k_2 and $\overline{x}$ is the amplitude over the cycle.

7. Algebraic Models

Given that the models raised for MR dampers are complex and computationally heavy, researchers have sought to provide simpler models. Earlier models predominantly stemmed from theoretical examinations of the device's behavior or that of its specific fluid. While these studies provided valuable insights, they often proved time-intensive and necessitated specialized expertise. In contrast, certain research groups prioritize operational and practical applications, striving to construct models that are as streamlined as possible, yet retain the fundamental and effective properties. These models serve a dual purpose: they facilitate the numerical simulation of devices in structural control and guide the management of the devices. However, MR dampers have high hysteresis and nonlinear behavior; therefore, the introduced models should show this phenomenon clearly and have sufficient accuracy. Algebraic

models are another possibility proposed by researchers. In this group of models, the hysteresis behavior of the damper is mainly expressed by simple algebraic expressions. The accuracy of these models is desirable to a large extent.

7.1. Weng Model. Weng et al. [96] presented a model employing an algebraic expression based on the arctangent function to simulate the hysteresis behavior of an MR damper. In this model, the employment of both the hyperbolic tangent function and the sign function successfully replicates the damper's behavior without resorting to differential relations, such as those found in the Bouc–Wen relation. The model introduced by them is given by the following equation:

$$F_d(t) = f_0 + c_b\dot{x}(t) + \frac{2}{\pi} f_y \arctan\{k[\dot{x}(t) - \dot{x}_0 \operatorname{sgn}(\ddot{x}(t))]\}, \tag{88}$$

where F_d is the restoring force of the MR damper, f_0 is the preload value owing to the nitrogen accumulator, c_b represents the viscous damping coefficients, and f_y is the yield force. Parameter k is a specific shape coefficient, and $\dot{x}_0$ is the hysteretic velocity. $\dot{x}$ and $\ddot{x}$ are the velocity and acceleration of the damper piston, respectively.

7.2. Cesmeci and Engin Model. Cesmeci and Engin [97] proposed a modified version of the Weng et al. [96] model. They found that Weng's model was in good agreement with the experimental data, except for the lower current inputs of the highest excitation velocity. This was possibly due to the fluid inertial force, which became more critical at lower input currents than the induced yield stress because the excitation acceleration increased. Therefore, to improve the model, they added an inertial force term to the following equation:

$$F_d(t) = f_0 + c_b\dot{x}(t) + \frac{2}{\pi} f_y \arctan\{k[\dot{x}(t) - \dot{x}_0 \operatorname{sgn}(\ddot{x}(t))]\} + m\ddot{x}(t). \tag{89}$$

Parameter m in (89) represents the virtual mass to be determined based on experimental data.

7.3. Metered Model. To enhance Weng's model, Metered et al. [98] incorporated amplitude and excitation frequency parameters. While these parameters increase the model's accuracy in predicting the damper's response to external excitation, they also constrain its application in structural control. This limitation arises because buildings are exposed to inherently random vibrations, making it challenging to reliably predict the excitation's amplitude and frequency. Their proposed model is given by the following equation:

$$F_d(t) = f_0 + c_b\dot{x}(t) + \frac{2}{\pi} f_y \arctan\{k[\dot{x}(t) - \dot{x}_0 \operatorname{sgn}(\ddot{x}(t))]\}(A_1 a + A_2)(F_1 f + F_2), \tag{90}$$

where a is the amplitude and f is the excitation frequency. Parameters A_1, A_2, F_1, and F_2 are constants obtained from the identification and curve-fitting processes.

7.4. Balamurgan Model. Based on their experimental results, Balamurgan et al. [99] found that an MR damper exhibited voltage-dependent nonlinear hysteresis behavior. However, any change in the input voltage has a visual effect on the postyield saturation peak force and magnitude of the hysteresis loop. They suggested that the resulting damping value could be expressed in a general form consisting of two independent functions: the control voltage of the device and hysteretic force.

$$F_d = F_i(v)F_h(x, \dot{x}, \ddot{x}). \tag{91}$$

In the above equation, F_i is a function of the voltage, which is shown by the parameter v, and F_h is a hysteretic function. Function F_i is a monotonous nonlinear incremental function of the voltage and can be used as a gain function. The nonlinear gradual behavior of F_i can be represented by an asymmetric sigmoid function that has a bias with the axis [100]. Equation (92) shows their proposed damper force.

$$F_d(t) = \left[f_0 + c_b\dot{x}(t) + \frac{2}{\pi} f_y \arctan\{k[\dot{x}(t) - \dot{x}_0 \operatorname{sgn}(\ddot{x}(t))]\}\right]\left(1 + \frac{k_2}{1 + e^{-a_2(\sigma/v_0 + I_0)}} - \frac{k_2}{1 + e^{-a_2 I_0}}\right), \tag{92}$$

where k_2 and a_2 are positive constant values, I_0 is an arbitrary constant value signifying bias, and v_0 is a constant. These parameters must be derived from measured data.

8. Hyperbolic Tangent-Function Models

Researchers have used the hyperbolic tangent function to express the hysteresis behavior of MR damper. However, exact classification of these models is difficult. Some of these models have been described in previous sections. In this section, the most effective hyperbolic model is presented.

8.1. Bass Model. The Bass hyperbolic tangent mode [102] consists of two sets of spring-dashpot elements connected by a mass element, as shown in Figure 30. The inertial-mass element resists motion through Coulomb friction. The displacement and velocity of the mass relative to the fixed base are denoted by x_0 and $\dot{x}_0$, respectively. The displacement and velocity of the damping piston relative to the mass are represented by x_1 and $\dot{x}_1$, respectively, and the general movement parameters of the damper are represented by x and $\dot{x}$, respectively, which are the result of adding these parameters with the correct sign.

Moreover, the parameters k_1 and c_1 model the preyield viscoelastic behavior model. The postyield viscoelastic behavior is represented by a spring (k_0) and a dashpot (c_0). m_0 denotes the inertial mass of both the fluid and piston, and f_0 is the yield force. V_{ref} is the reference velocity that affects the overall shape of the transition curve from the elastic to the plastic region of the function. The damper output force and dynamic characteristics of the system are presented as equations (87) and (88) in the state-space form.

$$\begin{bmatrix} \dot{x}_0 \\ \ddot{x}_0 \end{bmatrix} = \begin{bmatrix} 0 & 1 \\ \dfrac{(-k_0 - k_1)}{m_0} & \dfrac{(-c_0 - c_1)}{m_0} \end{bmatrix} \begin{bmatrix} x_0 \\ \dot{x}_0 \end{bmatrix} + \begin{bmatrix} 0 & 0 \\ \dfrac{k_1}{m_0} & \dfrac{c_1}{m_0} \end{bmatrix} \begin{bmatrix} x \\ \dot{x} \end{bmatrix} + \begin{bmatrix} 0 \\ \dfrac{1}{m_0} \end{bmatrix} f_0 \tanh\left(\frac{\dot{x}_0}{v_{\text{ref}}}\right), \tag{93}$$

$$F = \begin{bmatrix} -k_1 & -c_1 \end{bmatrix} \begin{bmatrix} x_0 \\ \dot{x}_0 \end{bmatrix} + \begin{bmatrix} k_1 & c_1 \end{bmatrix} \begin{bmatrix} x \\ \dot{x} \end{bmatrix}. \tag{94}$$

The model has unknown parameters in the form of first- and second-order polynomial functions. These parameters are current-dependent input operations, which are obtained from the identification of a specific MR damper device.

8.2. Kwok Model. Kwok et al. [101] proposed a model in which the hyperbolic tangent function was used to represent the MR damper hysteresis loop. Linear functions were used to show the conventional viscous damping and spring stiffness. The Kwok model can be expressed as follows:

$$F = kx + c\dot{x} + \alpha z + f_0 \text{ where } z = \tanh(\beta\dot{x} + \delta \operatorname{sgn}(x)). \tag{95}$$

In these equations, c and k are the viscous and stiffness coefficients, respectively; α is the hysteresis scale factor; z is the hysteresis variable given by the hyperbolic tangent function; and f_0 is the damper force offset. The components constituting the hysteresis curve are shown in Figure 31, [101]. These parameters describe the force-velocity response of the damper. The viscosity term $(c\dot{x})$ forms an inclined line that depicts the relationship between the velocity and the dissipating force of the damper in the postyield regions (at both ends of the hysteresis loop). k is responsible for opening the horizontal ellipse composed of kx, from the vicinity of the zero velocity. The parameter β forms the fundamental form of the hysteresis curve. This coefficient is the damping-velocity scale coefficient that defines the slope of the hysteresis loop. δ is a scale coefficient, and the sign of the displacement determines the width of the hysteresis loop using the $\delta \operatorname{sgn}(x)$ term. The overall hysteresis loop was scaled by the α coefficient, which determines the height of the hysteresis loop. In the original study, the unknown parameters of the model were identified using the PSO optimization algorithm [103].

Models employing the hyperbolic tangent function to articulate the internal dynamic behavior of the damper typically lack an intrinsic inverse model. Nevertheless, certain models can be streamlined based on the integration of the hyperbolic function within the model's final equation. In such cases, the hyperbolic tangent function is substituted with the sign function, facilitating the formulation of inverse function relationships. The Kwok model is a notable example within this category.

8.3. Yang Models. Yang et al. [104] worked on MR dampers that have a friction lagging effect in their force-velocity diagram. Figure 32 shows the force-velocity and force-displacement diagrams of the damper. They proposed a nonlinear algebraic hysteretic model for dampers, based on a hyperbolic function. The following equation represents this relationship:

$$F = kx + c\dot{x} + \alpha z \text{ where } z = \arctan(\beta\dot{x}) + \delta \operatorname{sgn}(x). \tag{96}$$

In these formulas, F is the damping force; $\dot{x}$ and x are the velocity and displacement of the piston, respectively; c is the viscous damping coefficient; k is the stiffness coefficient; and α is the hysteretic factor. Parameter z represents the internal dynamic effect of the device from the Coulomb damping force, which describes the hysteresis behavior of the force-

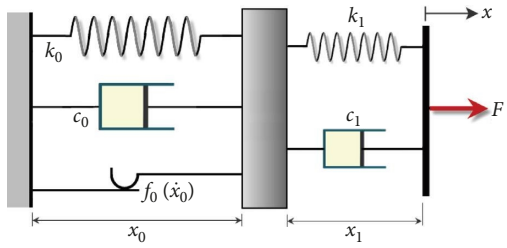

FIGURE 30: The Bass hyperbolic tangent function model (Section 8.1).

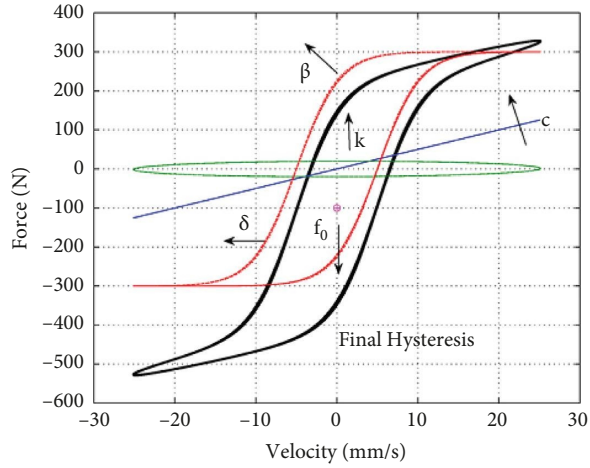

FIGURE 31: Hysteresis parameters of the Kwok model [101] (Section 8.2).

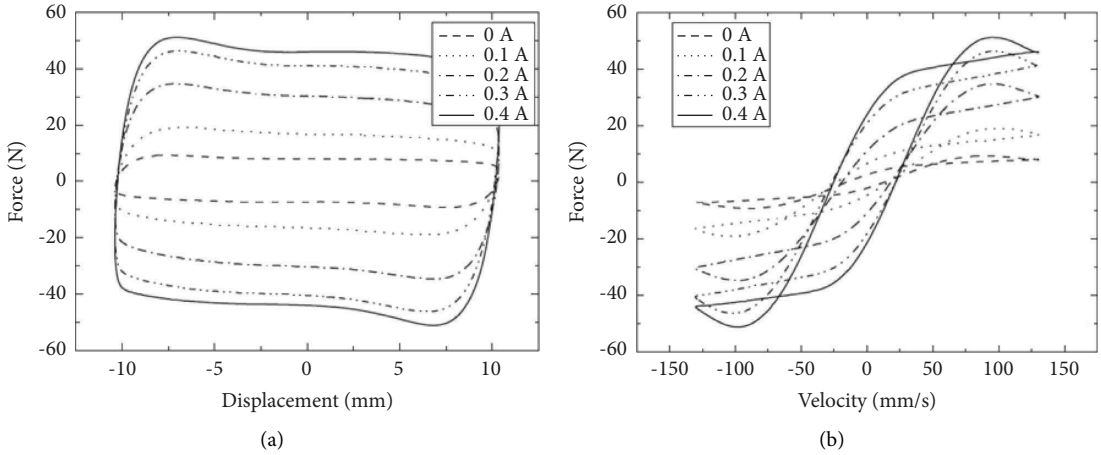

FIGURE 32: Variation of damping force with input current [104]: (a) force vs. displacement; (b) force vs. velocity (Section 8.3).

velocity loop. β and δ are the essential coefficients of the slope and the width of the hysteresis loop, respectively. These unknown parameters of the model are obtained from the identification process, which are linear or quadratic relationships of the damper input current.

In another study on MR dampers, Yang et al. [105] proposed a model in which a componentwise additive strategy, including viscous damping, spring, and a hysteretic component, was used. The damping force produced by this new model is expressed in the following equation:

$$F = kx + c_0\dot{x} + \frac{f_b}{e^{\alpha\dot{x}+\beta\mathrm{sgn}(x)} + \gamma} + f_0. \tag{97}$$

The parameters used in the above relation are known and accepted symbols in this field. Here, F is the damping force, $\dot{x}$ is the velocity, x is the displacement, c_0 is the viscous damping coefficient, and k is the stiffness coefficient. f_b, α, β,

and γ are the parameters describing the hysteresis characteristics of the device. Operator sgn(.) is the sign function, and f_0 is the offset of the damping force. The model parameters are linear and quadratic equations relative to the damper input-management current, which is derived from the identification process.

8.4. Cheng Models. In 2020, Cheng et al. [106] proposed a parametric model for MR dampers that considered the amplitude and frequency of excitation. The proposed model was a modified hyperbolic tangent model. The results show that the proposed model has higher fitting accuracy and can be well adapted to changing conditions. According to the type and size of the damper used and verification of parameters' sensitivity, the proposed model is as follows:

$$\begin{aligned} F_m &= c(I, A, f)\dot{x} + \alpha(I) z_m, \\ z_m &= \tanh\left(\beta(I, A, f)\dot{x} + \delta_c \operatorname{sgn}(x)\right), \end{aligned} \tag{98}$$

where $c(I, A, f)$ and $\beta(I, A, f)$ are functions of the current I and the excitation amplitude and frequency are denoted as A and f, respectively. $\alpha(I)$ is a function of the current.

Furthermore, the proposed model is invertible, allowing for tracking of the damping force. The authors endeavored to enhance result accuracy by elucidating the relationship between the damping force and the frequency of external excitation. Yet, as previously noted, the suitability of such a model for structural control fields, characterized by their randomness and nonharmonic nature, remains ambiguous.

9. Magic Formula

The *magic formula* offers an effective approximation for nonlinear curves [107]. Comprising a combination of various trigonometric functions, it is extensively utilized to estimate vehicle tire performance in mechanical simulations. Indeed, this model represents a specific application of the hyperbolic tangent function in terms that delineate and epitomize the internal dynamic performance of the damping device. The common *magic* formulation is

$$F = D \sin\{C \arctan[\beta(1 - E)\alpha + E \arctan(\beta\alpha)]\}, \tag{99}$$

where β, C, D, and E are the parameters that control the shape of the curve. α is an independent variable that can be selected from the main movement parameters of the device, such as displacement, velocity, and deflection angle, based on its actual responses. Pan et al. [107] showed that the acquired tire force-deflection angle curve is similar to the plastic-fluid curve of the MR damper, with some differences in describing the hysteresis characteristics. The magic formula representing the MR damper is given by

$$F_{\text{mfm}} = D \sin\{C \arctan[\beta(1 - E)(\dot{x} + A|x|) + E \arctan(\beta(\dot{x} + A|x|))]\} + k_c\dot{x} + kx + f_0. \tag{100}$$

In this equation, x represents the displacement and $\dot{x}$ represents the velocity for both damper pistons. The other parameters of the model are defined as follows: A is the hysteretic factor that determines the half-width of the MR damper hysteresis curve and is generally positive; β is generally a positive stiffness factor; C is a shape factor that determines the "S" curve shape and is approximately equal to 1; D is used as the peak factor and determines the damping-force saturation of the damper, which is generally a positive value; E is the curvature factor that determines the yield characteristics, which is typically less than 1; k_c is the viscous damping coefficient; k is the MR-damper stiffness coefficient; and f_0 is the bias force.

The parameters in this context can be chosen as constant, linear, or quadratic polynomials, depending on their dependency on the damper management current, a dependency that becomes evident postidentification. For parameters A and β, it is also possible to have a dependency on the amplitude and excitation frequency. This model can be inverted with the introduction of certain simplifications. The precision of the resultant inverse model is contingent upon the identified parameters and their relation to either the current or the amplitude and frequency of the external excitation.

10. Dynamic Models Based on the Dahl Hysteresis Operator

The Dahl model [108, 109] belongs to the first generation of dynamic-friction models. In addition to MR dampers, this model has been used in standard simulation models in the aerospace industry [110, 111]. The starting point of the model is as follows:

$$\frac{\mathrm{d}F(x)}{\mathrm{d}x} = \sigma_0 \operatorname{sgn}\left(1 - \operatorname{sgn}(\dot{x})\frac{F}{F_c}\right)\left|1 - \operatorname{sgn}(\dot{x})\frac{F}{F_c}\right|^i. \tag{101}$$

This form of the Dahl model was further developed and became a well-known equation, characterized by the following relations for better numerical implementation:

$$F(x) = \sigma_0 \check{z}; \dot{\check{z}} = \dot{x} \operatorname{sgn}\left(1 - \operatorname{sgn}(\dot{x})\frac{\sigma_0\check{z}}{F_c}\right)\left|1 - \operatorname{sgn}(\dot{x})\frac{\sigma_0\check{z}}{F_c}\right|^i. \tag{102}$$

The parameter definitions are defined as follows. F is the friction force; $\check{z}$ is the state variable interpreted as the elastic deformation of surface ruggedness of the adjacent bodies; $\dot{x}$ is the sliding velocity; x is the body displacement; σ_0 is the

rugged stiffness; i is the hysteresis loop-shape coefficient; and F_c is the Coulomb friction.

The most explicit form of the Dahl model is

$$F(x) = F_c z;\ \dot{z} = \rho(\dot{x} - |\dot{x}|z). \tag{103}$$

10.1. Modified Dahl Model. Figure 33 shows a modified Dahl model proposed by Zhou et al. [112] based on the experiments of Zhou [34], and Zhou et al. [113] performed on MR-damper devices. They found that the results could be represented in the form of a model based on the Dahl operator, which simulates the Coulomb friction force observed in the results.

$$F(x) = k_0 x + c_0 \dot{x} + f_d z - f_0, \tag{104}$$

where k_0 is the stiffness coefficient, c_0 is the viscous damping coefficient, f_d is the Coulomb force regulated by the applied magnetic field, z is the dimensionless hysteresis variable given by (103), and f_0 is the force exerted by the seals to measure the bias.

10.2. Viscous Dahl Model. Ikhouane et al. [59] proposed the viscous Dahl model to represent the dynamic nature of a shear-mode MR damper. This version of the Dahl model is expressed by the following equation:

$$F(x) = k_x(v)\dot{x}(t) + k_w(v)w(t), \tag{105}$$

where the constants k_x and k_w are voltage dependent and w is obtained from (43). Figure 34 illustrates this model schematically. This model was used in several studies [74, 75, 114, 115].

10.3. Asymmetric Dahl Model. Garcia et al. [116] tested a prototype of an MR damper whose force-displacement response curves and the force-velocity obtained were asymmetric. Hence, they proposed modifications to the Dahl viscous model to consider the effects of asymmetry on the behavior of the MR dampers. The force produced by the damper is as follows (105), and its viscosity and friction parameters are obtained from the following relationships:

$$\begin{cases} k_{w1}w(t), & \text{when } w(t) \geq 0, \\ k_{w2}w(t), & \text{when } w(t) \leq 0, \end{cases} \begin{cases} k_{x1}\dot{x}(t), & \text{when } \dot{x}(t) \geq 0, \\ k_{x2}\dot{x}(t), & \text{when } \dot{x}(t) \leq 0. \end{cases} \tag{106}$$

All the parameters (k_i) were obtained from the identification process.

11. General Dynamic Models

This section presents models that rely on the potential of identification methods developed in recent years for faster and more accurate identification of complex problems with increased unknowns. Shortly, a significant increase in this branch of research will occur to reproduce the numerical version of MR dampers.

In 2018, Zhao et al. [117] presented a dynamic hysteretic model to describe the force-velocity properties of MR dampers with various current excitations. It can be used to simulate the nonlinear properties of MR dampers more accurately. The model was presented using nonlinear state equations.

$$\dot{\eta} = k_i[U - \Delta(\eta)];\ \Phi(U) = \eta - aU + b;\ \Delta(\eta) = \begin{cases} k(\eta - x_0), & \text{when } \eta > x_0, \\ 0, & \text{when } |\eta| \leq x_{0,} \\ k(\eta + x_0), & \text{when } \eta < -x_{0.} \end{cases} \tag{107}$$

where U is the model input, η is a state variable, $\Phi(U)$ is the model output, a is the feedforward gain, k_i is an integration gain, and $\Delta(\eta)$ is the output of the dead-zone operator. b is the bias. x_0 and k_i can affect the width and amplitude of the hysteresis loop. Because of its dynamic nature, the model can represent the hysteresis of MR dampers. It provides a simple building block for developing various dynamic hysteretic models for MR dampers and represents a general framework. The structure of the model is shown in Figure 35.

In 2018, Zhao and Xu [118] proposed a model based on the sigmoid function that was based on a comparison of experimental data. The data used were predicted by the original sigmoid model and considered the Stribeck effect (Figure 36).

The model was designed to overcome the shortcomings of the original sigmoid model considering the properties of the MR damper, including the viscosity, elasticity, force hysteresis, and force mutation in the low-velocity region. This is formulated as follows:

$$F_{\text{sig}}^{\text{corr}} = F_{\text{ys}}\left(\frac{1 - e^{-\delta(\dot{x} - \dot{x}_h)}}{1 + e^{-\delta(\dot{x} - \dot{x}_h)}}\right) + \text{sgn}(\dot{x})F_{\text{sc}}\left(1 - e^{-|\dot{x}/\dot{x}_s|}\right) + k_0(x) + c_0(\dot{x}). \tag{108}$$

The parameters were identified using genetic algorithms. The results show that their model can well predict the Stribeck effect in the low-velocity region of small-scale dampers.

In 2018, Yuan et al. [119] proposed a model by combining the hyperbolic tangent and exponential functions. This model describes the nonlinear behavior of MR dampers as a simple parametric mode. The model typically consists of

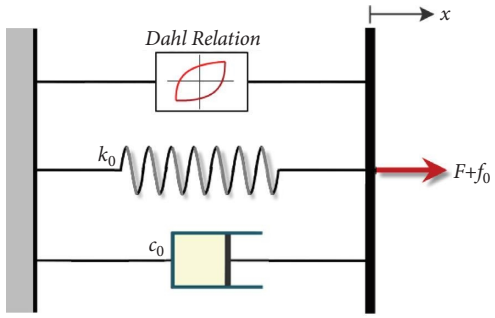

Figure 33: Modified Dahl model (Section 10.1).

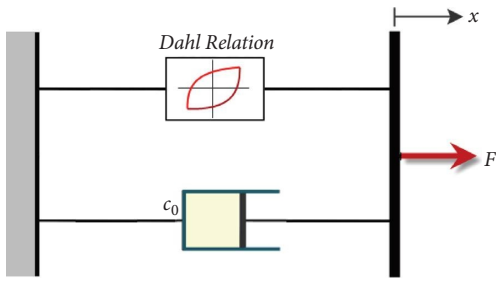

Figure 34: Viscous Dahl model (Section 10.2).

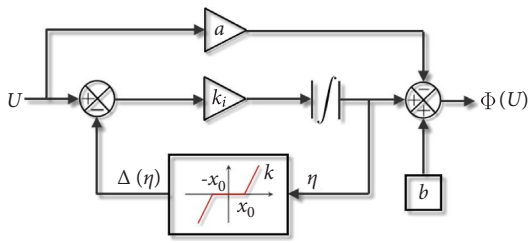

Figure 35: Zhao general dynamic model structure, 2018 (Section 11).

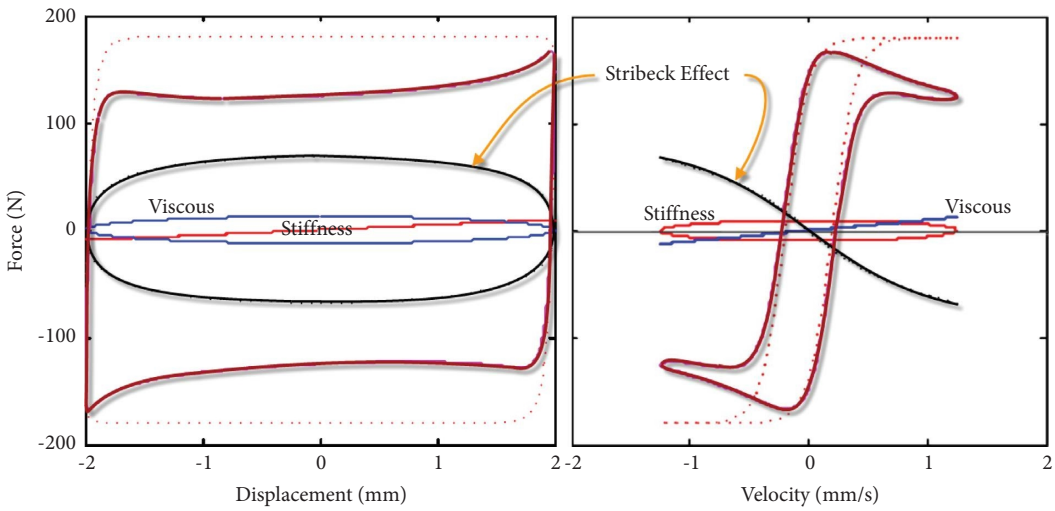

Figure 36: The Stribeck effect on the resulted curve [118] (Section 11).

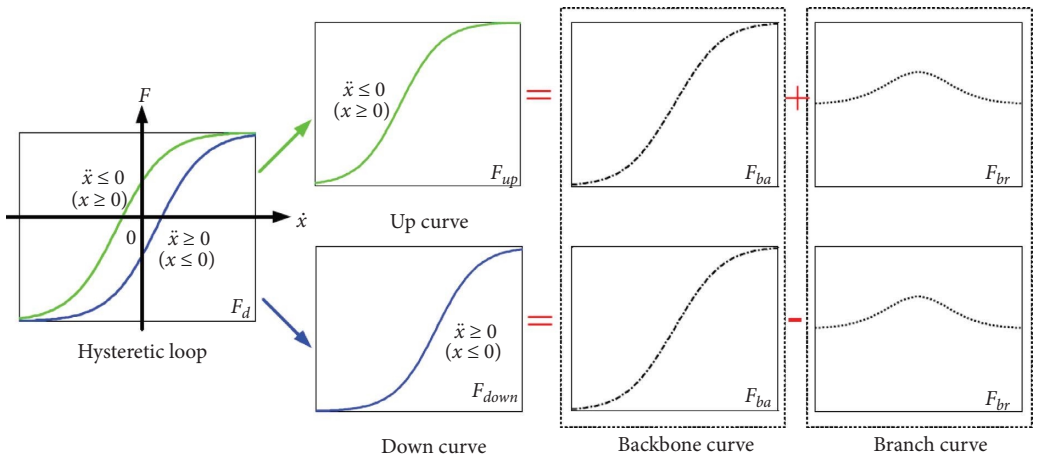

FIGURE 37: Details of the hysteresis division method: branch and backbone curve [120] (Section 11).

a hysteretic component, linear spring, viscous damper, and a fixed force value. The model is given by

$$F = \mathrm{VS}_1 C\eta e^{-A|\dot{x}|}\dot{x} + T(i)S_2 \tanh(\alpha\dot{x} + \beta x) + Kx + F_0, \tag{109}$$

where the constants $S1$ and $S2$ depend on the geometric and physical properties of the fluid MR, respectively. However, the model still requires scale parameters to match the numerical force-velocity curve with the corresponding curve results from laboratory tests.

Yu et al. [120] proposed a new model based on the hysteresis division method to describe the complex nonlinear behavior of an MR damper. This method divides the force-velocity hysteresis loop into a branch and backbone curve (Figure 37).

$$F_d = \begin{cases} F_{\mathrm{up}}, & \text{when } \ddot{x} \geq 0, \\ F_{\mathrm{down}}, & \text{when } \ddot{x} < 0, \end{cases} = \begin{cases} F_{\mathrm{ba}} + F_{\mathrm{br}}, & \ddot{x} \geq 0, \\ F_{\mathrm{ba}} - F_{\mathrm{br}}, & \ddot{x} < 0, \end{cases}$$
$$F_{\mathrm{ba}} = a\left(\frac{1 - e^{b\dot{x}\,\mathrm{sgn}(\dot{x})}}{1 + e^{c\dot{x}\,\mathrm{sgn}(\dot{x})}}\right)\mathrm{sgn}(\dot{x});\ F_{\mathrm{br}} = d \quad \exp\left\{-\left[\frac{\dot{x}\,\mathrm{sgn}(\dot{x}) - e}{f}\right]^2\right\}, \tag{110}$$

where $\dot{x}$ denotes the damper velocity and a, b, c, d, e, and f are the parameters that must be identified in association with the excitation. This model accurately describes the nonlinear hysteresis characteristics of small MR dampers. Moreover, it has a time-saving and efficient identification process and can be integrated into semiactive-vibration-control strategy. However, the performance of the model against nonharmonic excitation and its efficiency were not considered in their study.

In 2019, He et al. [121] proposed a mechanism-based unified MR-damper model based on a neuro-fuzzy technique to represent the direct dynamics of MR dampers. Based on kinetics and rheology, the damping force of an MR damper consists of the friction, elasticity, viscosity, inertia, and shear terms. The model parameters have unique physical meanings, and the model can be conveniently used for semiactive control in vehicle applications.

$$F = f + F_k + F_c + F_n + F_b,$$
$$f = \begin{cases} A & \ddot{x} > 0 \\ -A & \ddot{x} \leq 0 \end{cases};\ F_k = k(x - x_0);\ F_c = c\dot{x};\ F_n = n\ddot{x}, \tag{111}$$
$$F_b = D_b \quad \sin\left\{C_b \quad \arctan B_b\left[(1 - E_b)\dot{x} + \frac{E_b}{B_b} \quad \arctan(B_b\dot{x})\right]\right\} \text{ where: } C_b = 1 \pm \left(1 - \frac{2}{\pi}\arcsin\frac{Y_m}{D_b}\right).$$

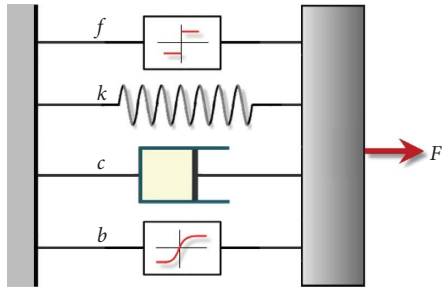

Figure 38: Mechanism-based unified MR-damper model (Section 11).

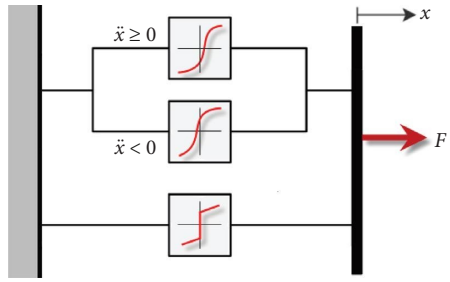

Figure 39: Quasistatic-magic-formula model (Section 11).

The authors used the "magic formula" to represent the shear behavior of the MR damper, F_b, which is similar to the slip behavior of tiers. They constructed an inverse model based on the adaptive neuro-fuzzy inference system (ANFIS) technique, and precise training data were obtained from the proposed unified hysteretic model. The simulation results demonstrate that the model can accurately and efficiently describe the direct dynamic characteristics of an MR damper. A schematic representation of the model is shown in Figure 38.

Bui et al. [122] proposed a novel parametric dynamic model based on a quasistatic model (QS) and hysteresis multiplier of the magic formula (Figure 39). Their model could effectively and accurately capture the strong nonlinear hysteresis phenomenon of MR dampers. The quasistatic-magic-formula (QSMF) model formulates both the shear and flow modes of MR dampers, and the asymmetric hysteresis responses of the damper are more accurate than those of the Spencer and Pan models.

$$F = F_{\mathrm{QS}} \quad \sin\{C \quad \arctan[B(1-E)z + E \quad \arctan(Bz)]\},$$
$$z = \begin{cases} \dot{x} + S_a x & \ddot{x} \geq 0 \\ \dot{x} + S_b x & \ddot{x} < 0 \end{cases}; \; F_{QS} = F_\eta + F_\tau + F_f. \tag{112}$$

Additionally, the QSMF-model parameters are easier to identify, and the model is feasible and applicable to semi-active control systems based on small-scale MR dampers.

12. Concluding Remarks

A successful control algorithm is based on a good sense of the seismic behavior of the structure and sufficient knowledge of control device operation. Much effort has been made to identify MR dampers as efficient but complicated tool; however, their complicated operation has also been noted. Various relationships have been proposed to describe the highly nonlinear behavior of these devices. An algorithm is more successful if the control device has clear management rules (inverse model) to act as a control and a regulative narrative. Therefore, proper identification of these devices alongside using the correct inverse model is essential. The selection of an appropriate mathematical model describing the device is important during the identification process. It is important to note that the first step in selecting an appropriate mathematical model always begins with laboratory samples. The response of a damper to changes in kinetic parameters, such as displacement and velocity, and changes in the damping force with changes in control factors, such as voltage or current, are essential.

The models discussed in this review are characterized by parametric relations. Researchers have employed various specific functions to depict the damper's behavior, resulting in a subset of models adept at accurately simulating the device's operation. These models can be broadly categorized into two distinct groups. The first encompasses models that depict the nonlinear internal dynamics of the damper, where a parameter is expressed through a differential formulation, exemplified by the Dahl or Bouc–Wen models. Despite their efficacy in simulating damper behavior, these models exhibit constraints in facilitating continuous damper control, making them more suited for bang-bang or clipped-control algorithms. Conversely, the second group leverages geometric and explicit functions, excelling in crafting inverted models. This permits designers to implement continuous control algorithms, achieving

a damping force closely aligned with the desired control force. However, the damper's response to variations in the amplitude and frequency of external stimuli warrants deeper investigation.

The research showcased here represents only a fraction of the extensive efforts made over the past decades to decipher the nonlinear behavior of MR dampers. These dampers stand out as one of the most effective and practical tools to enhance the seismic performance of structures. Our findings highlight several vital considerations:

(i) The model should be simple with a restrained number of parameters.

(ii) It must be capable of replicating the force-velocity cycle and the hysteresis behavior of the damper.

(iii) The performance of the proposed model, particularly in the transitional region around the yield stress, should be both accurate and closely approximated.

(iv) Ensuring the model's invertibility is paramount.

(v) The model parameters should be sufficiently flexible yet straightforward in illustrating the dependency of results on control factors, such as current or voltage.

Undoubtedly, what has been done thus far has been effective but not sufficient. The strong dependence of device segments on their physical properties prevents the provision of empirical and simple mathematical formulas. Therefore, continuous efforts are being made to identify the factors that affect the damping behavior of the device and to provide the most appropriate mathematical models that can express the complexity of the device response, particularly in areas where rheological fluid yields. At the first glance, the use of complex functions appears to be an effective way to identify MR dampers. However, it should be noted that the numerical reproduction of the damper response is only half that is required by the designer to design a successful and efficient control algorithm. The second is the management of the devices to increase the efficiency of the control configuration. Therefore, the proposed model should be simple, accurate, and efficient. This simplicity plays a crucial role in the implementation of the inverse model, which plays a significant role in controlling the device and generating the dissipating force closest to the required control force. The combination of these two parts is not simple in practice, and this is an issue that requires further research.

Data Availability

Corresponding data are not available for this review study. This is a so-called state-of-the-art document.

Conflicts of Interest

The authors declare that they have no conflicts of interest.

Authors' Contributions

All the authors contributed equally to this work.

Acknowledgments

This work was partially funded by the Spanish Agencia Estatal de Investigación (AEI), Ministerio de Economía, Industria y Competitividad (MINECO), and the Fondo Europeo de Desarrollo Regional (FEDER) through the research projects PID2021-122132OB-C21 and TED2021-129512B-I00 and by the Generalitat de Catalunya through the research project 2021-SGR-01044.

References

[1] F. Scozzese, L. Gioiella, A. Dall'Asta, L. Ragni, and E. Tubaldi, "Influence of viscous dampers ultimate capacity on the seismic reliability of building structures," *Structural Safety*, vol. 91, Article ID 102096, 2021.

[2] D. De Domenico, G. Ricciardi, and I. Takewaki, "Design strategies of viscous dampers for seismic protection of building structures: a review," *Soil Dynamics and Earthquake Engineering*, vol. 118, pp. 144–165, 2019.

[3] A. Pavia, F. Scozzese, E. Petrucci, and A. Zona, "Seismic upgrading of a historical masonry bell tower through an internal dissipative steel structure," *Buildings*, vol. 11, no. 1, p. 24, 2021.

[4] L. Ragni, F. Micozzi, E. Tubaldi, and A. Dall'Asta, "Seismic behaviour of a rc frame isolated by hdnr bearings under increasing intensity levels," in *Proceedings of the 7th International Conference on Computational Methods in Structural Dynamics and Earthquake Engineering Methods in Structural Dynamics and Earthquake Engineering*, Crete, Greece, June 2019.

[5] J. Rabinow, "The magnetic fluid clutch," *Electrical Engineering*, vol. 67, no. 12, pp. 1167–1315, 1948.

[6] G. Bossis, P. Khuzir, S. Lacis, and O. Volkova, "Yield behavior of magnetorheological suspensions," *Journal of Magnetism and Magnetic Materials*, vol. 258-259, no. 2, pp. 456–458, 2003.

[7] Lord Corporation, "Semi-active suspensions," 2023, https://www.lord.com/products-and-solutions/active-vibration-control/industrial-suspension-systems/magneto-rheological-mr-fluid.

[8] M. R. Jolly, J. W. Bender, and J. D. Carlson, "Properties and applications of commercial magnetorheological fluids," *Smart Structures and Materials 1998: Passive Damping and Isolation*, vol. 3327, pp. 262–275, 1998.

[9] M. R. Jolly, J. W. Bender, and J. D. Carlson, "Properties and applications of commercial magnetorheological fluids," *Journal of Intelligent Material Systems and Structures*, vol. 10, no. 1, pp. 5–13, 1999.

[10] J. Poynor, "*Innovative designs for magneto-rheological dampers*," M.S. thesis, Virginia Polytechnic Institute and State University, Blacksburg, VA, USA, 2001.

[11] M. Kciuk and R. Turczyn, "Properties and application of magnetorheological fluids," *Journal of Achievement in Material and Manufacturing Engineering*, vol. 18, no. 1-2, pp. 127–130, 2006.

[12] J. Huang, J. Q. Zhang, Y. Yang, and Y. Q. Wei, "Analysis and design of a cylindrical magneto-rheological fluid brake," *Journal of Materials Processing Technology*, vol. 129, no. 1-3, pp. 559–562, 2002.

[13] W. Klein, A. Mężyk, and M. Otorowski, "The application overhaul of magnetorheological fluids in mechanical

engineering," *International Scientific Conference TEMAG*, vol. 129, pp. 95–105, 2005.
[14] H. M. Chen, K. H. Tsai, G. Z. Qi, J. C. S. Yang, and F. Amini, "Neural network for structure control," *Journal of Computing in Civil Engineering*, vol. 9, no. 2, pp. 168–176, 1995.
[15] F. Pozo, L. Acho, A. Rodríguez, and G. Pujol, "Nonlinear modeling of hysteretic systems with double hysteretic loops using position and acceleration information," *Nonlinear Dynamics*, vol. 57, no. 1-2, pp. 1–12, 2009.
[16] B. F. Spencer Jr, S. J. Dyke, M. K. Sain, and J. D. Carlson, "Phenomenological model for magnetorheological dampers," *Journal of Engineering Mechanics*, vol. 123, no. 3, pp. 230–238, 1997.
[17] J. Gang, M. K. Sain, K. D. Pham, B. F. Spencer, and J. C. Romallo, "Modeling MR-dampers: a nonlinear blackbox approach," *American Control Conference*, vol. 1, pp. 429–434, 2001.
[18] Y. K. Wen, "Method for random vibration of hysteretic systems," *Journal of the Engineering Mechanics Division*, vol. 102, no. 2, pp. 249–263, 1976.
[19] R. C. Ehrgott and S. F. Masri, "Modelling the oscillatory dynamic behaviour of electrorheological materials in shear," *Smart Materials and Structures*, vol. 1, no. 4, pp. 275–286, 1992.
[20] W. H. Li, G. Z. Yao, G. chen, S. H. Yeo, and F. F. Yap, "Testing and steady state modeling of a linear MR damper under sinusoidal loading," *Smart Materials and Structures*, vol. 9, no. 1, pp. 95–102, 2000.
[21] T. Butz and O. von Stryk, "Modelling and simulation of electro- and magnetorheological fluid dampers," *ZAMM-Journal of Applied Mathematics and Mechanics/Zeitschrift für Angewandte Mathematik und Mechanik: Applied Mathematics and Mechanics*, vol. 82, no. 1, pp. 3–20, 2002.
[22] C. C. Chang and P. N. Roschke, "Neural network modeling of a magnetorheological damper," *Journal of Intelligent Material Systems and Structures*, vol. 9, no. 9, pp. 755–764, 1998.
[23] W. Sun, H. Hu, and J. Weng, "Design, testing and modeling of a magnetorheological damper with stepped restoring torque," *Journal of Intelligent Material Systems and Structures*, vol. 17, no. 4, pp. 335–340, 2006.
[24] M. Zapateiro and N. Luo, "Neural network modeling of a magnetorheological damper," *Artificial Intelligence Research and Development*, vol. 163, no. 9, pp. 351–358, 2007.
[25] K. C. Schurter and P. N. Roschke, "Neuro-fuzzy control of structures using magnetorheological dampers," *American Control Conference*, vol. 2, pp. 1097–1102, 2001.
[26] H. Du and N. Zhang, "Evolutionary takagi-sugeno fuzzy modelling for mr damper," in *Proceeding of the Sixth International Conference on Hybrid Intelligent Systems (HIS'06)*, Auckland, New Zealand, December 2006.
[27] Z. Q. Gu and S. O. Oyadiji, "Application of MR damper in structural control using ANFIS method," *Computers & Structures*, vol. 86, no. 3-5, pp. 427–436, 2008.
[28] J. D. Carlson and M. R. Jolly, "MR fluid, foam and elastomer devices," *Mechatronics*, vol. 10, no. 4-5, pp. 555–569, 2000.
[29] H. U. Oh, "Experimental demonstration of an improved magneto-rheological fluid damper for suppression of vibration of a space flexible structure," *Smart Materials and Structures*, vol. 13, no. 5, pp. 1238–1244, 2004.
[30] D. R. Gamota and F. E. Filisko, "Dynamic mechanical studies of electrorheological materials: moderate frequencies," *Journal of Rheology*, vol. 35, no. 3, pp. 399–425, 1991.
[31] N. M. Wereley, L. Pang, and G. M. Kamath, "Idealized hysteresis modeling of electrorheological and magnetorheological dampers," *Journal of Intelligent Material Systems and Structures*, vol. 9, no. 8, pp. 642–649, 1998.
[32] L. Pang, G. M. Kamath, and N. M. Wereley, "Analysis and testing of a linear stroke magnetorheological damper," in *Proceedings of the 39th AIAA/ASME/ASCE/AHS/ASC Structures, Structural Dynamics, and Materials Conference and Exhibit*, Long Beach, CA, USA, August 1998.
[33] R. A. Snyder, G. M. Kamath, and N. M. Wereley, "Characterization and analysis of magnetorheological damper behavior under sinusoidal loading," *AIAA Journal*, vol. 39, no. 7, pp. 1240–1253, 2001.
[34] Q. Zhou, "Two mechanic models for magnetorheological damper and corresponding test verification," *Earthquake Engineering and Engineering Vibration*, vol. 22, no. 4, pp. 144–150, 2002.
[35] A. Occhiuzzi, M. Spizzuoco, and G. Serino, "Experimental analysis of magnetorheological dampers for structural control," *Smart Materials and Structures*, vol. 12, no. 5, pp. 703–711, 2003.
[36] Z. X. Zhang and F. L. Huang, "A new magneticrheological damper nonlinear Bingham hysteretic model and ANSYS implementation," *Applied Mechanics and Materials*, vol. 351-352, pp. 1146–1151, 2013.
[37] S. Soltane, S. Montassar, O. Ben Mekki, and R. El Fatmi, "A hysteretic Bingham model for MR dampers to control cable vibrations," *Journal of Mechanics of Materials and Structures*, vol. 10, no. 2, pp. 195–206, 2015.
[38] T. C. Papanastasiou, "Flows of materials with yield," *Journal of Rheology*, vol. 31, no. 5, pp. 385–404, 1987.
[39] R. Bouc, "A Mathematical model for hysteresis," *Acta Acustica United with Acustica*, vol. 24, no. 1, pp. 16–25, 1971.
[40] Y. J. Park, Y. K. Wen, and A. H. Ang, "Random vibration of hysteretic systems under bi-directional ground motions," *Earthquake Engineering & Structural Dynamics*, vol. 14, no. 4, pp. 543–557, 1986.
[41] A. Domínguez, R. Sedaghati, and I. Stiharu, "Modelling the hysteresis phenomenon of magnetorheological dampers," *Smart Materials and Structures*, vol. 13, no. 6, pp. 1351–1361, 2004.
[42] A. Domínguez, R. Sedaghati, and I. Stiharu, "A new dynamic hysteresis model for magnetorheological dampers," *Smart Materials and Structures*, vol. 15, no. 5, pp. 1179–1189, 2006.
[43] A. Domínguez-González, I. Stiharu, and R. Sedaghati, "Practical hysteresis model for magnetorheological dampers," *Journal of Intelligent Material Systems and Structures*, vol. 25, no. 8, pp. 967–979, 2014.
[44] N. Ambhore, S. Hivarale, and D. Pangavhane, "A study of Bouc-Wen model of magnetorheological fluid damper for vibration control," *International Journal of Engineering Research and Technology*, vol. 2, no. 2, pp. 1–6, 2013.
[45] M. T. Braz César and R. Barros, "Experimental and numerical analysis of MR dampers," *Chinese Journal of Engineering*, vol. 2014, Article ID 915694, 7 pages, 2014.
[46] M. A. Razman, G. Priyandoko, and A. R. Yusoff, "Bouc-Wen model parameter identification for a MR fluid damper using particle swarm optimization," *Advanced Materials Research*, vol. 903, pp. 279–284, 2014.
[47] W. Liu, Y. Luo, B. Yang, and W. Lu, "Design and mechanical model analysis of magnetorheological fluid damper," *American Journal of Mechanics and Applications*, vol. 4, no. 1, pp. 15–19, 2016.

[48] G. Z. Yao, F. F. Yap, G. Chen, W. Li, and S. H. Yeo, "MR damper and its application for semi-active control of vehicle suspension system," *Mechatronics*, vol. 12, no. 7, pp. 963–973, 2002.

[49] S. J. Dyke, B. F. Spencer Jr, M. K. Sain, and J. D. Carlson, "An experimental study of MR dampers for seismic protection," *Smart Materials and Structures*, vol. 7, no. 5, pp. 693–703, 1998.

[50] S. J. Dyke, B. F. Spencer Jr, M. K. Sain, and J. D. Carlson, "Modeling and control of magnetorheological dampers for seismic response reduction," *Smart Materials and Structures*, vol. 5, no. 5, pp. 565–575, 1996.

[51] M. Giuclea, T. Sireteanu, D. Stancioiu, and C. W. Stammers, "Model parameter identification for vehicle vibration control with magnetorheological dampers using computational intelligence methods," *Proceedings of the Institution of Mechanical Engineers Part I: Journal of Systems & Control Engineering*, vol. 218, no. 7, pp. 569–581, 2004.

[52] G. Kumar, A. Kumar, and R. S. Jakka, "The particle swarm modified quasi bang-bang controller for seismic vibration control," *Ocean Engineering*, vol. 166, pp. 105–116, 2018.

[53] S. J. Dyke, B. F. Spencer Jr, M. K. Sain, and J. D. Carlson, "Seismic response reduction using magnetorheological dampers," *IFAC Proceedings*, vol. 29, no. 1, pp. 5530–5535, 1996.

[54] G. Yang, B. F. Spencer Jr, J. D. Carlson, and M. K. Sain, "Large-scale MR fluid dampers: modeling and dynamic performance considerations," *Engineering Structures*, vol. 24, no. 3, pp. 309–323, 2002.

[55] A. Spaggiari and E. Dragoni, "Efficient dynamic modelling and characterization of a magnetorheological damper," *Meccanica*, vol. 47, no. 8, pp. 2041–2054, 2012.

[56] F. Yi, S. J. Dyke, J. M. Caicedo, and J. D. Carlson, "Seismic response control using smart dampers," *American Control Conference*, vol. 2, pp. 1022–1026, 1999.

[57] L. M. Jansen and S. J. Dyke, "Semiactive control strategies for MR dampers: comparative study," *Journal of Engineering Mechanics*, vol. 126, no. 8, pp. 795–803, 2000.

[58] F. Yi, S. J. Dyke, J. M. Caicedo, and J. D. Carlson, "Experimental verification of multiinput seismic control strategies for smart dampers," *Journal of Engineering Mechanics*, vol. 127, no. 11, pp. 1152–1164, 2001.

[59] F. Ikhouane and S. J. Dyke, "Modeling and identification of a shear mode magnetorheological damper," *Smart Materials and Structures*, vol. 16, no. 3, pp. 605–616, 2007.

[60] G. Yang, B. F. Spencer, H. J. Jung, and J. D. Carlson, "Dynamic modeling of large-scale magnetorheological damper systems for civil engineering applications," *Journal of Engineering Mechanics*, vol. 130, no. 9, pp. 1107–1114, 2004.

[61] Y. K. Lau and W. H. Liao, "Design and analysis of a magnetorheological damper for train suspension," *Smart Structures and Materials 2004: Damping and Isolation*, vol. 5386, pp. 214–225, 2004.

[62] Y. K. Lau and W. H. Liao, "Design and analysis of magnetorheological dampers for train suspension," *Proceedings of the Institution of Mechanical Engineers, Part F: Journal of Rail and Rapid Transit*, vol. 219, no. 4, pp. 261–276, 2005.

[63] G. Tsampardoukas, C. W. Stammers, and E. Guglielmino, "Hybrid balance control of a magnetorheological truck suspension," *Journal of Sound and Vibration*, vol. 317, no. 3-5, pp. 514–536, 2008.

[64] S. F. Ali and A. Ramaswamy, "Testing and modeling of MR damper and its application to SDOF systems using integral backstepping technique," *Journal of Dynamic Systems, Measurement, and Control*, vol. 131, no. 2, Article ID 021009, 2009.

[65] A. Dominguez, R. Sedaghati, and I. Stiharu, "Semi-active vibration control of adaptive structures using magnetorheological dampers," *AIAA Journal*, vol. 44, no. 7, pp. 1563–1571, 2006.

[66] A. Dominguez, R. Sedaghati, and I. Stiharu, "Modeling and application of MR dampers in semi-adaptive structures," *Computers & Structures*, vol. 86, no. 3-5, pp. 407–415, 2008.

[67] X. Q. Ma, S. Rakheja, and C. Y. Su, "Development and relative assessments of models for characterizing the current dependent hysteresis properties of magnetorheological fluid dampers," *Journal of Intelligent Material Systems and Structures*, vol. 18, no. 5, pp. 487–502, 2007.

[68] N. M. Kwok, Q. P. Ha, M. T. Nguyen, J. Li, and B. Samali, "Bouc–Wen model parameter identification for a MR fluid damper using computationally efficient GA," *ISA Transactions*, vol. 46, no. 2, pp. 167–179, 2007.

[69] M. Ismail, F. Ikhouane, and J. Rodellar, "The hysteresis Bouc–Wen model, a survey," *Archives of Computational Methods in Engineering*, vol. 16, no. 2, pp. 161–188, 2009.

[70] F. Ikhouane and J. Rodellar, "On the hysteretic bouc–wen model, Part I: forced limit cycle characterization," *Nonlinear Dynamics*, vol. 42, no. 1, pp. 63–78, 2005.

[71] F. Ikhouane and J. Rodellar, "On the hysteretic bouc–wen model, Part II: robust parametric identification," *Nonlinear Dynamics*, vol. 42, no. 1, pp. 79–95, 2005.

[72] F. Ikhouane and J. Rodellar, "On the hysteretic Bouc-Wen model, Part II: robust parametric identification," *The Shock and Vibration Digest*, vol. 38, no. 4, pp. 369-370, 2006.

[73] F. Ikhouane and O. Gomis-Bellmunt, "A limit cycle approach for the parametric identification of hysteretic systems," *Systems & Control Letters*, vol. 57, no. 8, pp. 663–669, 2008.

[74] A. R. Tsouroukdissian, F. Ikhouane, J. Rodellar, and N. Luo, "Modeling and identification of a small-scale magnetorheological damper," *Journal of Intelligent Material Systems and Structures*, vol. 20, no. 7, pp. 825–835, 2009.

[75] A. Rodríguez, N. Iwata, F. Ikhouane, and J. Rodellar, "Model identification of a large-scale magnetorheological fluid damper," *Smart Materials and Structures*, vol. 18, no. 1, Article ID 015010, 2008.

[76] A. Bahar, F. Pozo, L. Acho, J. Rodellar, and A. Barbat, "Parameter identification of large-scale magnetorheological dampers in a benchmark building," *Computers & Structures*, vol. 88, no. 3-4, pp. 198–206, 2010.

[77] A. Bahar, F. Pozo, L. Acho, J. Rodellar, and A. Barbat, "Hierarchical semi-active control of base-isolated structures using a new inverse model of magnetorheological dampers," *Computers & Structures*, vol. 88, no. 7-8, pp. 483–496, 2010.

[78] X. X. Bai, P. Chen, and L. J. Qian, "Principle and validation of modified hysteretic models for magnetorheological dampers," *Smart Materials and Structures*, vol. 24, no. 8, Article ID 085014, 2015.

[79] C. Canudas de Wit, H. Olsson, K. J. Åström, and P. Lischinsky, "A new model for control of systems with friction," *IEEE Transactions on Automatic Control*, vol. 40, no. 3, pp. 419–425, 1995.

[80] L. Alvarez and R. Jiménez, "Real-time identification of magneto-rheological dampers," *IFAC Proceedings*, vol. 35, no. 1, pp. 193–198, 2002.

[81] C. Sakai, H. Ohmori, and A. Sano, "Modeling of MR damper with hysteresis for adaptive vibration control," *IEEE*

International Conference on Decision and Control, vol. 4, pp. 3840–3845, 2003.

[82] P. Palka and M. Maślanka, "Inverse LuGre model for a small-scale MR damper," in *Proceedings of the 14th International Carpathian Control Conference (ICCC)*, pp. 284–287, Rytro, Poland, May 2013.

[83] R. Stanway, J. L. Sproston, and A. K. El-Wahed, "Applications of electro-rheological fluids in vibration control: a survey," *Smart Materials and Structures*, vol. 5, no. 4, pp. 464–482, 1996.

[84] H. Liu and J. Teng, "Modeling of smart dampers for vibration control," in *Proceedings of the 2004 International Conference on Intelligent Mechatronics and Automation*, pp. 177–181, Chengdu, China, August 2004.

[85] M. S. Seong, S. B. Choi, and C. H. Kim, "Damping force control of frictionless MR damper associated with hysteresis modeling," *Journal of Physics: Conference Series*, vol. 412, no. 1, Article ID 012044, 2013.

[86] D. H. Wang and W. H. Liao, "Magnetorheological fluid dampers: a review of parametric modelling," *Smart Materials and Structures*, vol. 20, no. 2, Article ID 023001, 2011.

[87] W. L. Ang, W. H. Li, and H. Du, "Experimental and modelling approaches of a MR damper performance under harmonic loading," *Journal of the Institution of Engineers*, vol. 44, no. 4, pp. 1–14, 2004.

[88] N. D. Sims, N. J. Holmes, and R. Stanway, "A unified modelling and model updating procedure for electro-rheological and magnetorheological vibration dampers," *Smart Materials and Structures*, vol. 13, no. 1, pp. 100–121, 2004.

[89] K. D. Weiss, J. D. Carlson, and D. A. Nixon, "Viscoelastic properties of magneto-and electro-rheological fluids," *Journal of Intelligent Material Systems and Structures*, vol. 5, no. 6, pp. 772–775, 1994.

[90] M. R. Jolly, J. D. Carlson, and B. C. Muñoz, "A model of the behaviour of magnetorheological materials," *Smart Materials and Structures*, vol. 5, no. 5, pp. 607–614, 1996.

[91] G. M. Kamath and N. M. Werely, "Nonlinear viscoelastic-plastic mechanisms-based model of an electrorheological damper," *Journal of Guidance, Control, and Dynamics*, vol. 20, no. 6, pp. 1125–1132, 1997.

[92] G. M. Kamath and N. M. Wereley, "A nonlinear viscoelastic–plastic model for electrorheological fluids," *Smart Materials and Structures*, vol. 6, no. 3, pp. 351–359, 1997.

[93] N. M. Wereley, G. M. Kamath, and V. Madhavan, "Hysteresis modeling of semi-active magnetorheological helicopter dampers," *Journal of Intelligent Material Systems and Structures*, vol. 10, no. 8, pp. 624–633, 1999.

[94] G. M. Kamath, N. M. Wereley, and M. R. Jolly, "Characterization of magnetorheological helicopter lag dampers," *Journal of the American Helicopter Society*, vol. 44, no. 3, pp. 234–248, 1999.

[95] Z. Li, Y. Q. Ni, H. Dai, and S. Ye, "Viscoelastic plastic continuous physical model of a magnetorheological damper applied in the high speed train," *Science China Technological Sciences*, vol. 56, no. 10, pp. 2433–2446, 2013.

[96] J. S. Weng, H. Y. Hu, and M. K. Zhang, "Experimental modeling of magnetorheological damper," *Journal of Vibration Engineering*, vol. 13, no. 4, pp. 616–621, 2000.

[97] S. Cesmeci and T. Engin, "Modeling and testing of a field-controllable magnetorheological fluid damper," *International Journal of Mechanical Sciences*, vol. 52, no. 8, pp. 1036–1046, 2010.

[98] H. Metered, S. Mostafa, S. El-Demerdash, N. Hammad, and M. El-Nashar, *Testing, Modelling and Analysis of a Linear Magnetorheological Fluid Damper under Sinusoidal Conditions*, SAE International, Warrendale, PA, USA, 2013.

[99] L. Balamurugan, J. Jancirani, and M. A. Eltantawie, "Generalized magnetorheological (MR) damper model and its application in semi-active control of vehicle suspension system," *International Journal of Automotive Technology*, vol. 15, no. 3, pp. 419–427, 2014.

[100] E. R. Wang, X. Q. Ma, S. Rakhela, and C. Y. Su, "Modelling the hysteretic characteristics of a magnetorheological fluid damper," *Proceedings of the Institution of Mechanical Engineers Part D: Journal of Automobile Engineering*, vol. 217, no. 7, pp. 537–550, 2003.

[101] N. M. Kwok, Q. P. Ha, T. H. Nguyen, J. Li, and B. Samali, "A novel hysteretic model for magnetorheological fluid dampers and parameter identification using particle swarm optimization," *Sensors and Actuators A: Physical*, vol. 132, no. 2, pp. 441–451, 2006.

[102] B. J. Bass and R. E. Christenson, "System identification of a 200 kN magneto-rheological fluid damper for structural control in large-scale smart structures," in *Proceedings of the 2007 American Control Conference*, pp. 2690–2695, New York, NY, USA, August 2007.

[103] J. Kennedy and R. Eberhart, "Particle swarm optimization," *International Conference on Neural Networks*, vol. 4, pp. 1942–1948, 1995.

[104] M. G. Yang, Z. Q. Chen, and X. G. Hua, "An experimental study on using MR damper to mitigate longitudinal seismic response of a suspension bridge," *Soil Dynamics and Earthquake Engineering*, vol. 31, no. 8, pp. 1171–1181, 2011.

[105] M. G. Yang, C. Y. Li, and Z. Q. Chen, "A new simple nonlinear hysteretic model for MR damper and verification of seismic response reduction experiment," *Engineering Structures*, vol. 52, pp. 434–445, 2013.

[106] M. Cheng, Z. Chen, W. Liu, and Y. Jiao, "A novel parametric model for magnetorheological dampers considering excitation characteristics," *Smart Materials and Structures*, vol. 29, no. 4, Article ID 045002, 2020.

[107] W. Pan, Z. Yan, J. Lou, and S. Zhu, "Research on MRD parametric model based on magic formula," *Shock and Vibration*, vol. 2018, Article ID 1871846, 10 pages, 2018.

[108] P. R. Dahl, "A solid friction model," in *Report Tor-0158(3107-18)-1. The Aerospace Corporation*, The Aerospace CorporationThe Aerospace Corporation, El Segundo, CA, USA, 1968.

[109] P. R. Dahl, "Solid friction damping of mechanical vibrations," *AIAA Journal*, vol. 14, no. 12, pp. 1675–1682, 1976.

[110] V. Lampaert, J. Swevers, and F. Al-Bender, "Comparison of model and non-model based friction compensation techniques in the neighbourhood of pre-sliding friction," *American Control Conference*, vol. 2, pp. 1121–1126, 2004.

[111] T. Piatkowski, "Dahl and LuGre dynamic friction models the analysis of selected properties," *Mechanism and Machine Theory*, vol. 73, pp. 91–100, 2014.

[112] Q. Zhou, S. R. K. Nielsen, and W. L. Qu, "Semi-active control of three-dimensional vibrations of an inclined sag cable with magnetorheological dampers," *Journal of Sound and Vibration*, vol. 296, no. 1-2, pp. 1–22, 2006.

[113] Q. Zhou, S. R. K. Nielsen, and W. L. Qu, "Semi-active control of shallow cables with magnetorheological dampers under harmonic axial support motion," *Journal of Sound and Vibration*, vol. 311, no. 3-5, pp. 683–706, 2008.

[114] N. Aguirre, F. Ikhouane, J. Rodellar, D. Wagg, and S. Neild, "Modeling and identification of a small scale magnetorheological damper," *IFAC Proceedings Volumes*, vol. 43, no. 10, pp. 19–24, 2010.

[115] N. Aguirre, F. Ikhouane, J. Rodellar, and R. Christenson, "Parametric identification of the Dahl model for large scale MR dampers," *Structural Control and Health Monitoring*, vol. 19, no. 3, pp. 332–347, 2012.

[116] I. García-Baños, F. Ikhouane, and N. Aguirre-Carvajal, "An asymmetric-friction based model for magnetorheological dampers ∗ ∗Supported by the Spanish Ministry of Economy, Industry and Competitiveness through grant DPI2016-77407-P (AEI/FEDER, UE)," *IFAC-PapersOnLine*, vol. 50, no. 1, pp. 14076–14081, 2017.

[117] X. Zhao, W. Qin, S. Wu, and H. Pan, "A dynamic hysteresis model for MR dampers based on particle swarm optimization," in *Proceedings of the 2018 IEEE 8th Annual International Conference on CYBER Technology in Automation, Control, and Intelligent Systems (CYBER)*, pp. 395–398, Tianjin, China, July 2018.

[118] Y. L. Zhao and Z. D. Xu, "A hysteretic model considering Stribeck effect for small-scale magnetorheological damper," *Smart Materials and Structures*, vol. 27, no. 6, Article ID 065021, 2018.

[119] X. Yuan, T. Tian, H. Ling, and T. Y. Qiu, "A new model for characterizing nonlinear hysteresis of magnetorheological fluid damper," *International Journal of Acoustics and Vibration*, vol. 24, no. 4, pp. 784–791, 2019.

[120] J. Yu, X. Dong, and Z. Zhang, "A novel model of magnetorheological damper with hysteresis division," *Smart Materials and Structures*, vol. 26, no. 10, Article ID 105042, 2017.

[121] Y. He, G. Liang, B. Xue, Z. Peng, and Y. Wei, "A unified MR damper model and its inverse characteristics investigation based on the neuro-fuzzy technique," *International Journal of Applied Electromagnetics and Mechanics*, vol. 61, no. 2, pp. 225–245, 2019.

[122] Q. D. Bui, X. X. Bai, and Q. Hung Nguyen, "Dynamic modeling of MR dampers based on quasi–static model and Magic Formula hysteresis multiplier," *Engineering Structures*, vol. 245, Article ID 112855, 2021.